Quantifying the role of the eddy transfer coefficient in simulating the response of the Southern Ocean Meridional Overturning Circulation to enhanced westerlies in a coarse-resolution model

Yiwen Li[1,2], Hailong Liu[1,2,3*], Pengfei Lin[1,2], Eric P. Chassignet[4], Zipeng Yu[1,2], Fanghua Wu[5]

[1]State Key Laboratory of Numerical Modeling for Atmospheric Sciences and Geophysical Fluid Dynamics (LASG), Institute of Atmospheric Physics, Chinese Academy of Sciences, Beijing 100029, China

[2]College of Earth and Planetary Sciences, University of Chinese Academy of Sciences, Beijing 100049, China

[3]Center for Ocean Mega-Science, Chinese Academy of Sciences, Qingdao 266071, China

[4]Center for ocean-Atmospheric Prediction Studies, Florida State University, Tallahassee 32306, Florida

[5]China Meteorological Administration, Beijing 100081, China

* Corresponding author: Hailong Liu (lhl@lasg.iap.ac.cn)

Abstract

The ability of a coarse-resolution ocean model to simulate the response of the Southern Ocean Meridional Overturning Circulation (MOC) to enhanced westerlies is evaluated as a function of the eddy transfer coefficient (κ), which is commonly used to parameterize the bolus velocities induced by unresolved eddies. By comparing five different schemes for κ, it is shown that a stratification-dependent and spatiotemporally varying coefficient leads to the largest response of the eddy-induced MOC (accounts for 82% of the reference eddy-resolving simulation). By decomposing the eddy-induced velocity into a new term derived from the κ's vertical variation (VV) and an already existing term based on the κ's spatial structure (SS), the largest response of the eddy compensation is attributed to the significantly intensified SS term, while the VV term weakens the response. Even though the parameterized eddy compensation response is traced back to the response of the isopycnal slope for all five experiments, the comparison between constant and spatiotemporally varying κ indicates that the larger κ is the direct factor leading to the stronger eddy compensation response. However, the stratification-dependent κ, especially its temporal variation, strengthens the eddy compensation response to enhanced westerlies by affecting the response of the isopycnal slope, which is a secondary impact of κ.

Keywords: the eddy transfer coefficient; mesoscale eddies parameterization; enhanced westerlies; Southern Ocean meridional overturning circulation; ocean model

1. Introduction

The Southern Ocean crucially connects the Atlantic, Pacific, and Indian Oceans through its meridional overturning circulation (MOC) and the Antarctic Circumpolar Current (ACC). It is also full of mesoscale eddies, which can significantly affect the Southern Ocean by altering the volume transport (Gent, 2016), the water mass formation (Waugh, 2014), and the carbon absorption (Swart et al., 2014). The Southern Ocean MOC consists of two cells: the upper cell and the lower cell. The upper cell involves both the upwelling of North Atlantic deep waters and the wind-induced northward surface Ekman transport. According to satellite data and atmospheric reanalysis (Swart and

Fyfe, 2012; Bracegirdle et al., 2013; Farneti et al., 2015), the Southern Hemisphere westerlies shifted poleward and intensified by ~20% due to anthropogenic global warming and stratospheric ozone depletion (Gent, 2016). Based on the wind-driven circulation theory, the intensified westerlies should enhance the circulations in the Southern Ocean, but the isopycnal slope from the Argo observation (Böning et al., 2008) does not show a corresponding enhancement. The reason is that the input energy from the wind is compensated by mesoscale eddies in the Southern Ocean, which absorb energy from the westerlies and are also enhanced by the intensification of the westerlies (Viebahn and Eden, 2010; Hofmann and Maqueda, 2011; Downes and Hogg, 2013). The eddy compensation can further affect the Southern Ocean sea surface temperature (SST) by dampening its response to enhanced westerlies (Doddridge et al., 2019). Thus, the Southern Ocean eddy compensation and its response to changes in the westerlies have a crucial role in the state of the Southern Ocean.

The simulation of eddy compensation in climate models requires eddy parameterization. Most climate models still use non-eddy-resolving ocean models, which means that eddy-induced transport must be parameterized. The parameterization is commonly done using the diffusivity (Redi, 1982) and bolus velocities (Gent and McWilliams, 1990, hereafter referred to as GM), or the skewness flux (Griffies, 1998), with an eddy transfer coefficient (κ). However, GM only parameterizes the transient eddy, so the eddy compensation referred to here is the transient eddy compensation. To properly parameterize the eddy compensation, κ should be variable in both space and time (Gent, 2016). This has been reported from the analysis of multiple non-eddy-resolving simulations with different ocean models, including the mixing length scheme (Visbeck et al., 1997; Eden and Greatbatch, 2008) and the buoyancy-dependent scheme (Ferreira et al., 2005). Hofmann and Maqueda (2011) show that the spatio-temporal variation of κ based on the mixing-length scale is important in parameterizing the eddy compensation. Gent and Danabasoglu (2011) emphasize the vertical variation of the buoyancy frequency dependent κ. Abernathey et al. (2011) found that κ should be proportional to the square root of the wind stress based on a zonal channel model with idealized geometry. While previous studies have indicated the importance of considering both the spatial and temporal variations of κ in simulating the eddy compensation, it is not clear which variation has the greater impact. Additionally, the impact of the additional vertical variation has only been examined using a buoyancy-dependent scheme of κ (Gent and Danabasoglu, 2011). Further investigation with different schemes of κ is necessary to clarify the role of the different characters of κ and the different schemes of κ in the simulation of eddy compensation.

The simulation of eddy compensation in coarse-resolution models requires spatiotemporal variation in κ. However, previous studies have shown inconsistent magnitudes of eddy compensation in response to changes in wind stress. For instance, Hofmann and Maqueda (2011) show a 67% increase in the eddy-induced MOC with doubled westerlies and a length-scale-dependent scheme for κ, while Gent and Danabasoglu (2011) show a 60% increase with only 50% enhanced westerlies using a buoyancy-dependent scheme. Furthermore, Downes et al. (2018) find a spread in the simulated trends of the eddy-induced MOC among 12 COERII models with different schemes for κ. To understand the spread of eddy compensation in coarse-resolution models, it is necessary to compare the results of different models and schemes. The high-resolution model is usually used as a reference to evaluate the spread, as most state-of-the-art eddy-resolving ocean models can resolve the impact of mesoscale eddies on the MOC response. The idealized channel model by Abernathey et al. (2011) and the eddy-resolving model by Meredith et al. (2012) both indicate a linear response of the eddy-induced MOC to wind stress. Bishop et al. (2016) show a 22.8% increase in the eddy-induced MOC (transient eddy-induced MOC) with a 50% increase in wind stress using an eddy-resolving coupled model. To determine the crucial features of κ for parameterizing the mesoscale eddies, it is helpful to compare high-resolution and low-resolution configurations of a single model, as this approach avoids the effects of different models' dynamic cores. This evaluation will also help determine which features of κ are important for parameterizing the eddy compensation in coarse-resolution models.

This study quantifies the response of the Southern Ocean MOC to increased westerlies in an ocean model that incorporates parameterized eddy effects through different schemes for κ. An eddy-resolving configuration serves as a reference for assessing the effects of different κ on the simulated eddy compensation. Two widely used κ schemes are considered: one depending on the buoyancy frequency from Ferreira et al. (2005), and another that incorporates time and length scales provided by the Eady growth rate, the Rossby radius of deformation, and the Rhines scale from Eden and Greatbatch (2008). Our findings reveal the following: (1) the largest simulated eddy compensation response among the coarse-resolution experiments using different κ represents 82% of the response from the reference eddy-resolving experiment, (2) the new term introduced by the vertical variation of κ reduces the eddy compensation response to enhanced westerlies, and (3) the stratification-dependent κ, particularly its temporal variation, enhances the eddy compensation response to enhanced westerlies by affecting the response of the isopycnal slope.

The remainder of the paper is organized as follows. Section 2 describes the ocean model, experiments, and methods of decomposing the eddy-resolving output into the eddy-induced and Eulerian mean transports. In section 3, the response of the circulation to the intensified westerlies in the eddy-resolving model and the coarse-resolution model with different κ are investigated. Section 4 describes how the eddy compensation response in the Southern Ocean is influenced by κ. The last section is the summary and discussion.

2. Experiments and methods

2.1 Eddy-resolving experiment

The ocean model used in this paper was developed at the State Key Laboratory of Numerical Modeling for Atmospheric Sciences and Geophysical Fluid Dynamics (LASG), Institute of Atmospheric Physics (IAP), and named the LASG/IAP Climate system Ocean Model (LICOM). The eddy-resolving experiment uses LICOM version

2.0 (LICOM2.0, Liu et al., 2012), with a 0.1° × 0.1° horizontal grid and 55 vertical levels. In the upper 300 m, 36 levels are used with an average layer thickness of less than 10 m. Biharmonic viscosity and diffusivity schemes are used in the momentum and tracer equations, respectively. The model domain covers 79°S–66°N, excluding the Arctic Ocean. There is a 5° buffer zone at 66°N, where temperature and salinity are restored to the climatological monthly temperature and salinity (Levitus and Boyer, 1994). The experiment, called LICOMH hereafter, was conducted after a 13-year spin-up and using the 60-year (1948-2007) daily Coordinated Ocean-Ice Reference Experiments (CORE, Large and Yeager, 2004) interannually varying forcing. Please refer to Yu et al. (2012) and Liu et al. (2014) for the details of the model description and basic performances.

2.2 Coarse-resolution experiments

The coarse resolution experiments use version 3.0 of LICOM (LICOM3, Lin et al., 2020; Li et al., 2020), which is coupled to the Community Ice Code version 4 (CICE4) through the NCAR flux coupler version 7 (CPL7), with approximately 1° horizontal resolution and 30 vertical levels. The vertical resolution is uniform in the top 150 m, with a grid spacing of 10 m, whereas the spacing is uneven below 150 m. The horizontal model grid uses a tripole grid (Murray, 1996) with two poles in the Northern Hemisphere, which are located at 65°N, 30°W and 65°N, 150°E, respectively. The tidal mixing parameterization scheme of St. Laurent et al. (2002) is implemented. The coarse-resolution experiments (hereafter referred to as LICOML) follow the second phase of the Coordinated Ocean-Ice Reference Experiments (COREII) protocol, forced by six-hourly atmospheric data and the bulk formula of Large and Yeager (2009). These experiments are integrated for 124 years, with two 62-year CORE-II cycles, and the second cycle is used for analysis here. The strength of the residual MOC, defined as the maximum positive value in the entire area, demonstrates similar trends and variability between the two cycles, except for the first 12 years. The trend of residual MOC from the second cycle is comparable to that from the eddy-resolving experiment, making the comparison between the coarse-resolution simulations and the eddy-resolving simulation valid, despite the skipping of the 12 years at the beginning of the cycle from coarse-resolution experiments and the 13-year spin-up from the eddy-resolving experiment.

There are five coarse-resolution experiments with different schemes for κ (listed in Table 1) to evaluate the influence of κ. The first two experiments, referred to as K500 and K1000, use constant κ of 500 m^2 s^{-1} and 1000 m^2 s^{-1}, respectively. The next two experiments (called FMH3D and FMH4D respectively) use an eddy transfer coefficient scheme based on the structure of buoyancy frequency as described in Ferreira et al. (2005):

$$\kappa = \frac{N^2}{N_{\mathrm{ref}}^2}\kappa_{\mathrm{ref}} \tag{1}$$

where κ is the eddy transfer coefficient, κ_{ref} is constant and set to 4000 m^2 s^{-1}, N^2 is the buoyancy frequency, and N_{ref}^2 is the reference buoyancy frequency at the bottom of the mixed layer. FMH4D uses a spatiotemporally varying κ, which follows Eq. (1). In FMH3D, its κ is the time-averaged κ during 1948-2009 from FMH4D, making it a control experiment to investigate the impact of the additional temporal variation of κ.

Table 1. The configurations of the experiments

Experiment	Resolutions (°)	κ (m^2/s)	Periods	Forcing
LICOMH	0.1	-	1949-2007	CORE II
K500	1	500	1948-2009	CORE II
K1000	1	1000	1948-2009	CORE II
FMH3D	1	$\overline{\kappa_{ref}(N^2/N_{ref}^2)}$	1948-2009	CORE II
FMH4D	1	$\kappa_{ref}(N^2/N_{ref}^2)$	1948-2009	CORE II
EG	1	$\alpha\sigma(x,y,z)L^2(x,y,z)$	1948-2009	CORE II

The fifth coarse-resolution experiment uses the scheme of κ from Eden and Greatbatch (2008), which is computed from time and length scales derived from the Eady growth rate, the Rossby radius of deformation, and the Rhines scale:

$$\kappa = \alpha\sigma(x,y,z)L^2(x,y,z) \quad (2)$$

$$\sigma = \frac{f|u_z|}{N} \quad (3)$$

where σ denotes an inverse eddy timescale that is given by the Eady growth rate, which is calculated by Eq. (3); L is an eddy length scale, which is the minimum of the local Rossby radius of deformation and the Rhines scale; and α is a constant parameter of order one following Eden and Greatbatch (2008) and Eden et al. (2009). The experiment is called EG hereafter.

Despite previous studies indicating that the isopycnal diffusivity is influenced by wind stress (Abernathey and Ferreira, 2015) and the diffusivity coefficient (also known as Redi coefficient, Abernathey and Marshall, 2013) can impact the Southern Ocean MOC in ocean models (Marshall et al., 2017), the focus of this study is solely on investigating the impact of the eddy transfer coefficient (also known as the GM coefficient). In all coarse-resolution experiments, the Redi coefficient is held constant at a value of 500 $m^2\ s^{-1}$.

2.3 Decomposition of MOC in LICOMH

The total MOC, also named the residual MOC, consists of the Eulerian and the eddy-induced MOC. Following Poulsen et al. (2018), the eddy-induced MOC in LICOMH is defined by the deviation of the total MOC from the Eulerian MOC calculated based on time-mean velocities. As in previous studies, we perform the decomposition analysis in the isopycnal coordinate system (e.g., Hallberg and Gnanadesikan, 2006; Munday et al., 2013; Bishop et al., 2016; Poulsen et al., 2018).

The residual MOC over a specified period is given by:

$$\psi(y,\sigma)_{res}^{High} = -\overline{\int_{west}^{east}\int_{z:\rho(x,y,z,t)\leq\sigma} v\,dz\,dx} \quad (4)$$

where $\psi(y,\sigma)_{res}^{High}$ is the residual MOC at a given potential density surface σ across a given latitude y. v is the meridional velocity transferred in density coordinates. dz is the density thickness, which is the product of $d\rho$ and $dz/d\rho$. x, y, and z are the usual cartesian coordinates. And $\rho(x, y, z, t)$ is the potential density, which is calculated with a reference pressure of 2000 dbar. The zonal integration here is from the west to the east and the potential density layers smaller than the given potential density σ are integrated with the vertical direction. $\overline{(\,)}$ denotes the average operator over time (ten years used here).

To obtain the Eulerian MOC, the decomposition is applied to the monthly velocity over a specified period in density coordinates. As mentioned by Poulsen et al. (2018), the time scale of the monthly outputs is enough to calculate the eddy-induced circulation. First, the velocity is transferred in density coordinates. Then, the time average (ten years used here) is applied to those velocities, resulting in a time-mean field over that period and its monthly deviation. Taking the meridional velocity as an example, we define the decomposition as follows:

$$v(x, y, \rho, t) = \bar{v}(x, y, \rho) + v^*(x, y, \rho, t) \tag{5}$$

where $\bar{v}$ is the time-mean meridional velocity and v^* is the deviation. The streamfunction derived from the time-mean field represents the Eulerian mean overturning circulation over that period, which includes the standing eddy. The formula is given by:

$$\psi(y, \sigma)_{Euler}^{High} = -\int_{west}^{east} \int_{\bar{z}:\overline{\rho(x,y,z,t)} \leq \sigma} \bar{v}\,dz\,dx \tag{6}$$

where $\psi(y, \sigma)_{Euler}^{High}$ is the Eulerian MOC at a given potential density surface σ across a given latitude y. $\bar{v}$ is the time-mean velocity in density coordinates over a specified period (ten years). dz is the product of $d\rho$ and $dz/d\rho$. x, y, and z are the usual cartesian coordinates. And $\overline{\rho(x, y, z, t)}$ is the time-mean potential density. The zonal integration here is from the west to the east and the time-mean potential density layers smaller than the given potential density σ are integrated with the vertical direction.

Finally, the difference between the residual MOC (ψ_{res}) and the Eulerian MOC (ψ_{Euler}) is the eddy-induced MOC:

$$\psi(y,\sigma)^{*\,High} = \psi(y,\sigma)^{High}_{res} - \psi(y,\sigma)^{High}_{Euler} \quad (7)$$

which captures the motion that varies on a temporal timescale shorter than the period of the applied time-averaging operator (ten years used here). And the eddy-induced MOC here only represents the MOC induced by the transient eddy.

2.4 Decomposition of MOC in LICOML

The decomposition of MOCs in coarse-resolution simulations (LICOML) is different from LICOMH, since the mesoscale eddy is not resolved in LICOML. For the coarse-resolution simulations, the residual MOC ($\psi(y,\sigma)^{Low}_{res}$) over a specified period, which is the same as that for the eddy-resolving simulation, is calculated based on the monthly output of the meridional velocity transferred in the density coordinate. The formula is as follows:

$$\psi(y,\sigma)^{Low}_{res} = -\overline{\int_{west}^{east}\int_{z:\rho(x,y,z,t)\le\sigma} v dz dx} \quad (8)$$

where $\psi(y,\sigma)^{Low}_{res}$ is the residual MOC for low-resolution simulations at a given potential density surface σ across a given latitude y. v is the simulated residual meridional velocity transferred in density coordinates. dz is the thickness of the density layers, which is the product of $d\rho$ and $dz/d\rho$ and a crucial component of the MOC. x, y, and z are the usual cartesian coordinates. And $\rho(x,y,z,t)$ is the potential density, which is calculated with a reference pressure of 2000 dbar. The zonal integration here is from the west to the east and the potential density layers smaller than the given potential density σ are integrated in the vertical direction. $\overline{(\ )}$ denotes the average operator over time, which is ten years here.

However, calculations of the Eulerian MOC and the eddy-induced MOC in LICOML are different from those for LICOMH. The eddy-induced MOC for the coarse-resolution simulation is derived from the monthly parameterized eddy-induced velocity. The formula is as follows:

$$\psi(y,\sigma)^{*Low} = -\overline{\int_{west}^{east}\int_{z:\rho(x,y,z,t)\le\sigma} v^* dz dx} \quad (9)$$

where $\psi(y,\sigma)^{*Low}$ is the eddy-induced MOC for low-resolution simulations. v^* is the parameterized eddy-induced meridional velocity. x, y, z, $\rho(x, y, z, t)$ and dz are the same as those in Eq. (7). The zonal integration is also from the west to the east and the potential density layers smaller than the given potential density σ are integrated in the vertical direction. $\overline{(\,)}$ also denotes the average operator over time, which is 10 years here. Then, the Eulerian MOC for low-resolution simulations is as follows:

$$\psi(y,\sigma)_{Euler}^{Low} = \psi(y,\sigma)_{res}^{Low} - \psi(y,\sigma)^{*Low} \quad (10)$$

where $\psi(y,\sigma)_{Euler}^{Low}$ is the Eulerian MOC at a given potential density surface σ across a given latitude y.

3. Responses to enhanced westerlies

3.1 Enhanced westerlies

Figure 1a shows the 12-month running mean monthly series of the zonal wind stress averaged in the Southern Ocean (40–60°S and 0–360°E) and its linear trend for LICOML. The wind stress was computed using CORE II forcing and model-predicted SST, which indicates an increasing trend from 1949 to 2007 with a magnitude of about 0.007 Pa/decade (significant by Mann–Kendall non-parametric test of the significance level of 95%). The trend is consistent with the enhanced westerlies in the Southern Ocean that appeared during recent decades found in previous studies (Swart and Fyfe, 2012; Bracegirdle et al., 2013; Farneti et al., 2015; Gent, 2016). The difference in the zonal wind stress between 1998–2007 and 1960–1969 is presented in Figure 1b. There is a general enhancement of the zonal wind stress in the Southern Ocean with a maximum of 0.1 Pa and about a 25.2% increase of the strength, which is defined by averaging over 40–60°S and 0–360°E. Furthermore, a slightly poleward shift of the zonal wind stress is also shown, which is confirmed by previous studies (e.g., Goyal et al., 2021). This significant multidecadal intensification of westerlies in the Southern Ocean is believed to be driven partially by ozone depletion and global warming (Thompson and Solomon, 2002; Marshall, 2003; Miller et al., 2016).

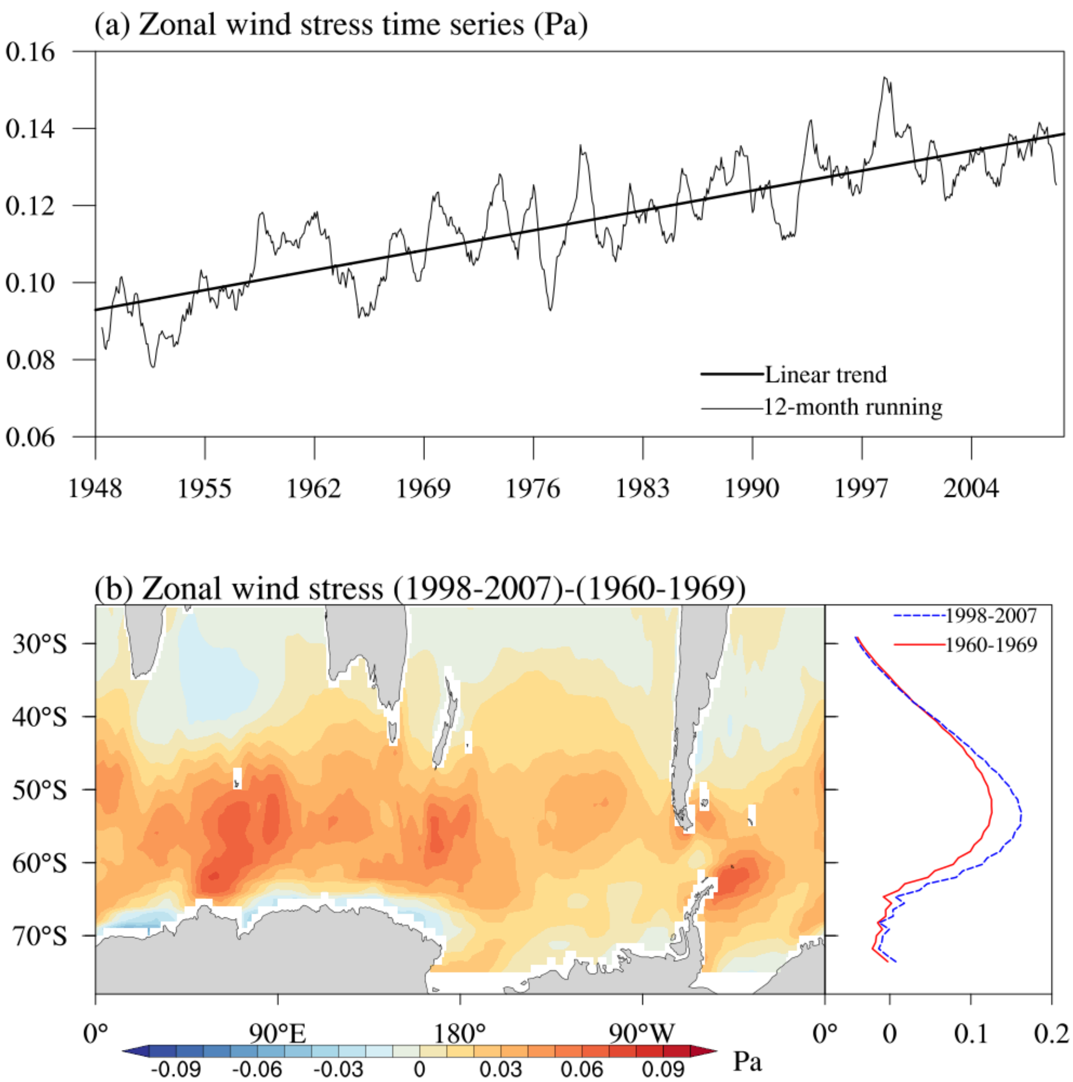

Figure 1. (a) The black line is the 12-month running mean zonal wind stress averaged in the Southern Ocean (40°S–60°S and 0–360°E) from LICOML. The thick black line is the linear trend of the monthly series. (b) The differences of the zonal wind stress from LICOML between periods of 1998–2007 and 1960–1969, and the zonally averaged values. The red solid and blue dashed lines are for 1960–1969 and 1998–2007, respectively.

The linear trend of the zonal wind stress in the Southern Ocean from LICOMH is almost the same as that from LICOML with a magnitude of 0.007 Pa/decade (Fig. S1). For the comparison between the two periods, LICOMH shows an increase in strength of 23.6%, which is 1.6% weaker than the 25.2% from LICOML. That offset comes from both the surface forcing and the feedback from simulated surface speed. The former is mainly due to the mapping process. Therefore, the latter factor may dominate the differences. In addition, the simulated sea surface temperature may also lead to differences through the calculation of the drag coefficient. However, the zonal wind stress trends between LICOMH and LICOML are almost the same (0.007 Pa/decade for both). Thus, in terms of the response of MOC to intensified westerlies, the difference in the wind stress magnitude between LICOMH and coarse-resolution simulations can be ignored. In general, the enhanced westerlies are well simulated in both LICOML and LICOMH (Fig. S1).

3.2 Response in the eddy-resolving experiment

The response of the Southern Ocean MOC to the intensified westerlies is estimated by the eddy-resolving experiment (LICOMH), in which mesoscale eddies can be resolved explicitly. The first row of Figure 2 shows the residual, Eulerian, and eddy-induced MOC in the isopycnal coordinate system during 1949–2007 in the Southern Ocean. The positive upper cell and the negative lower cell are presented clearly in the residual MOC (Fig. 2a). They are located from 35°S to 55°S near the surface of 36.45 kg m^{-3} and from 35°S to 75°S near the surface of 36.90 kg m^{-3}, respectively. This structure is in line with the theoretical pattern in the isopycnal coordinate system (Farneti et al., 2015). The eddy-induced MOC shows the opposite direction to the Eulerian MOC, compensating for the Eulerian MOC and leading to a weaker clockwise residual MOC in the upper cell, which is consistent with previous studies (e.g., Hallberg and Ganadesikan, 2006; Meredith et al., 2012; Paulsen et al., 2018).

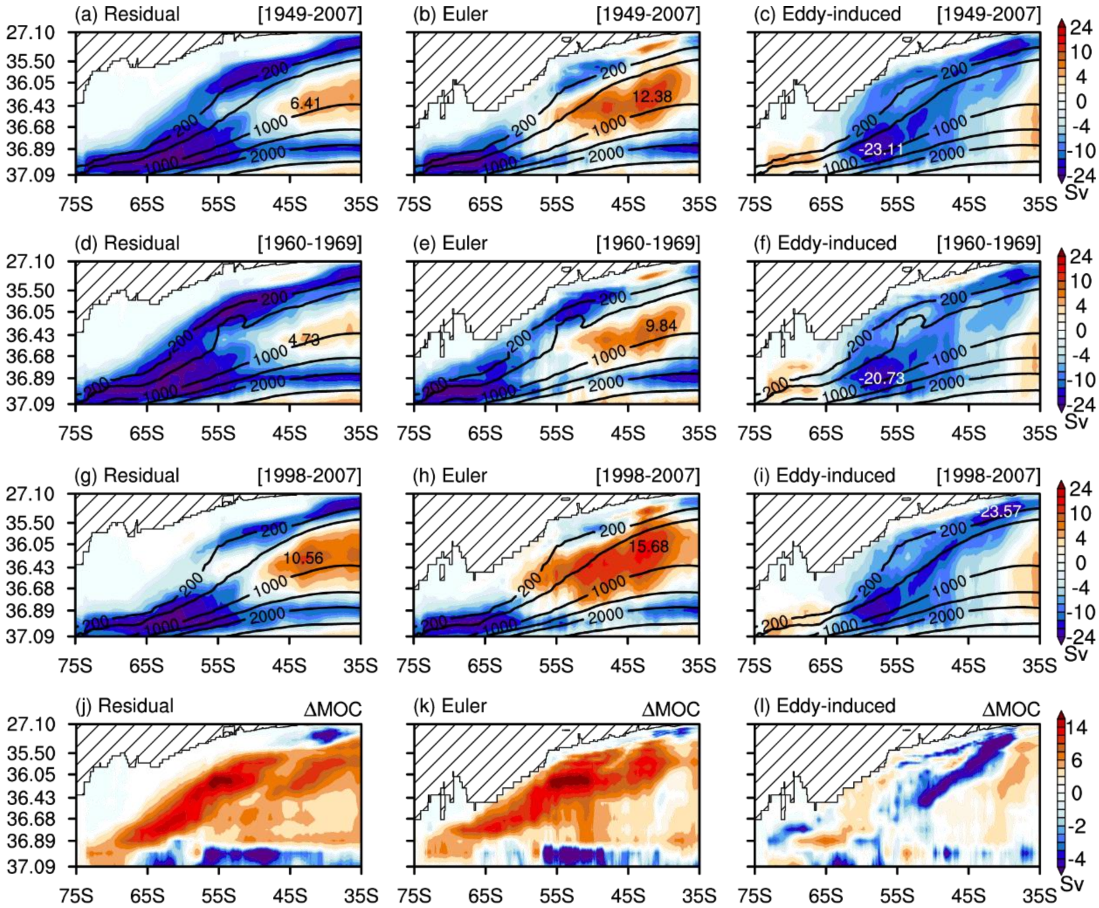

Figure 2. The first column is the MOC of residual currents for the periods of (a) 1949–2007, (d) 1960–1969, (g) 1998–2007, and (j) the difference between 1998–2007 and 1960–1969 for LICOMH in the isopycnal coordinate. The black curves represent the zonally averaged isobaths (200, 400, 1000, 1500, 2000, and 3000 m) in the isopycnal coordinate. The second and third columns are the same as the first column, but for the Eulerian MOC and the eddy-induced MOC, respectively. The black numbers in the first and second columns are the maximum of the closed residual and Eulerian MOC. The white numbers in the third column are the minimum of the eddy-induced MOC. (Unit: Sv)

The MOC during 1960–1969 and 1998–2007 is presented in the second and third rows of Figure 2 to evaluate the response of the MOC to enhanced westerlies. To quantify the response, we define the maximal positive value in the whole area as an index to measure the strength of the upper cell, which can represent the total north/south transport in the upper overturning cell at a certain latitude. The clockwise residual MOC during 1998–2007 (Fig. 2g) has a strength of 10.56 Sv, whereas it is 4.73 Sv during 1960–1969 (Fig. 2d), indicating a 5.83 Sv increase of the clockwise residual MOC from 1960–1969 to 1998–2007. That increase in the strength of the residual MOC (Fig. 2j and Table. 2) takes up to 123% compared with that from 1960–1969. For the Eulerian MOC in LICOMH, its enhancement is larger than that of the residual MOC, with a strength of 5.84 Sv (Fig. 2k and Table. 2), increasing by 59% compared with 1960–1969. The ratio of 59% is not in line with the ratio of the enhanced westerlies (25.2%), which may be caused by the changing isopycnal slope and standing eddies in the Eulerian MOC.

The distinction between the residual and the Eulerian MOC responses can be seen in the compensation effect of the eddy-induced MOC. As illustrated in Figure 2, the direction of the eddy-induced MOC (Fig. 2c, 2f, and 2i) is opposite to that of the Eulerian MOC (Fig. 2b, 2e, and 2h) in the region of the upper cell. Additionally, the eddy-induced MOC displays an increase in intensity over time (Fig. 2l). To further quantify this response, the minimum value in the whole area is defined as the strength of the eddy-induced MOC, which can represent the total north/south transport at a certain latitude. The strength is found to be -20.73 Sv during the period 1960-1969 and -23.57 Sv during the period 1998-2007. The intensified eddy-induced MOC, referred to as the eddy compensation response, has a strength of 2.84 Sv, constituting 13.7% of the eddy-induced MOC during 1960-1969. This ratio is smaller than that of the intensified westerlies (23.6%). This disparity may be caused by the varying isopycnal slope across the Southern Ocean, since the intensified wind stress leads to an increase of a similar magnitude in the overturning with the assumption of a largely invariant isopycnal slope field across the Southern Ocean (Meredith et al., 2012).

Based on the climatological MOCs and their response to changes, there are two categories of eddy compensation. The first category, referred to as simply "eddy compensation", encompasses the spatial compensation of the MOC. The second category, referred to as the "response of eddy compensation", encompasses both the spatial and temporal compensation, taking into account the enhancement of the Eulerian MOC as a result of strengthened westerlies.

3.3 Responses in the coarse-resolution experiments

To assess the efficacy of the parameterized eddy in the coarse-resolution ocean experiments, we examine five different experiments, which are schemes K500, K1000, FMH3D, FMH4D, and EG, each with a different scheme for κ (Fig. 3d, 3h, 3l, 3p, and 3t). As shown in Figure 3, the climatological mean eddy-induced MOC (the third column) of all five experiments shows anticlockwise circulations during 1948–2009, which is contrary to the Eulerian MOC (the second column). A change in the κ value from 500 $m^2\ s^{-1}$ to 1000 $m^2\ s^{-1}$ is expected to result in a stronger eddy-induced MOC (Fig. 3c and 3g). The patterns of the residual MOC in experiments with spatially varying κ (Fig. 3i, 3p, and 3t) show only slight differences compared to K1000, a result of the compensation between the Eulerian MOC and the eddy-induced MOC. While the climatological residual MOC is barely sensitive to the κ scheme, there are much larger Eulerian and eddy-induced MOCs differences between experiments with constant κ and experiments with spatially varying κ. The dependence of the eddy-induced MOC and the Eulerian MOC on the κ scheme may significantly impact the response of the residual MOC to the enhanced westerlies.

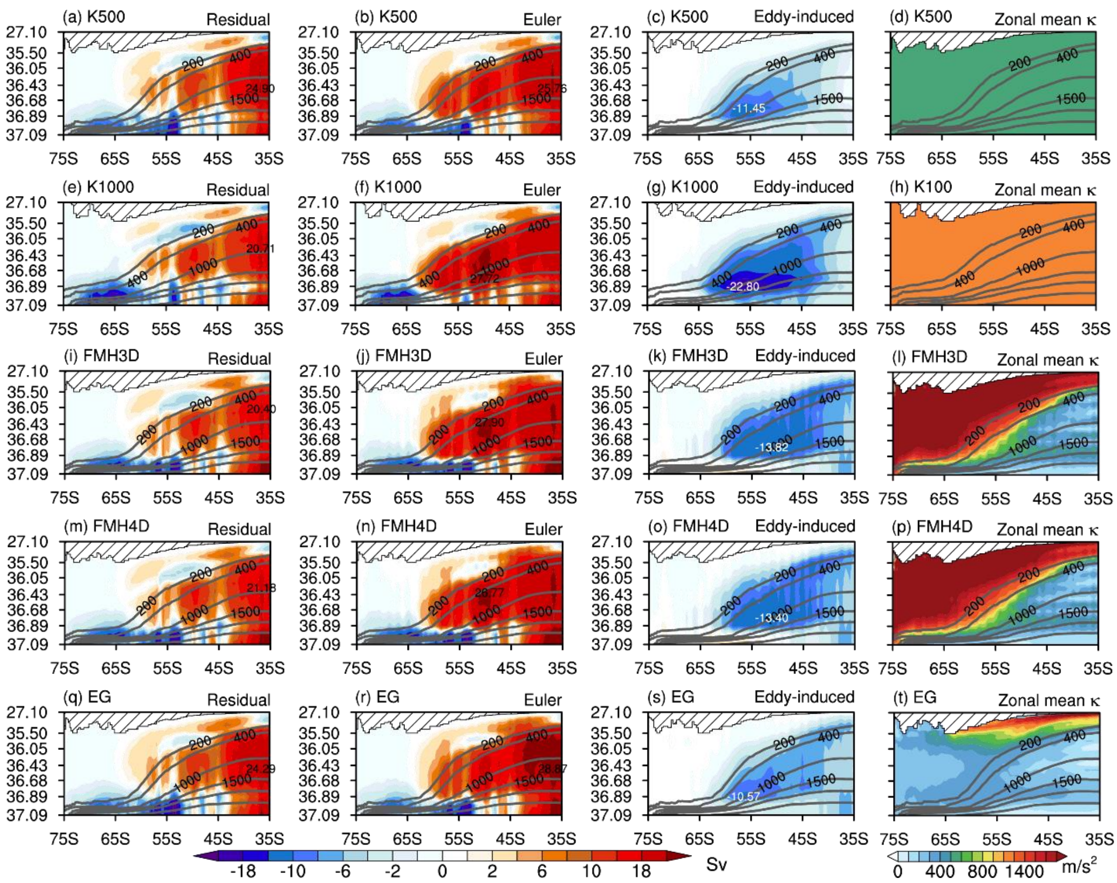

Figure 3. The top panels are (a) the residual MOC, (b) the Eulerian MOC, (c) the eddy-induced MOC, and (d) the eddy transfer coefficient (κ) for the K500 experiment during 1948–2009. The second to the bottom rows are the same as the first row, but for the K1000, FMH3D, FMH4D, and EG experiments, respectively. The gray lines represent the zonally averaged isobaths (200, 400, 1000, 1500, 2000, and 3000 m) in the isopycnal coordinate system. The black numbers in the first and second columns are the maximum of the residual and Eulerian MOC. The white numbers in the third column are the minimum of the eddy-induced MOC. (Unit: Sv)

Figure 4 shows the responses of the residual, Eulerian, and eddy-induced MOC between 1960–1969 and 1998–2007, in which there is an approximately 25.2% enhancement of westerlies in the Southern Ocean. From the first column of Figure 4, it can be seen that there are obvious differences among the responses of the residual MOC in the five experiments with different κ schemes. Furthermore, the changes in the residual MOC in all five experiments (first column in Fig. 4) are smaller than that of the Eulerian MOC (second column in Fig. 4), which is caused by the compensation of the enhanced anticlockwise eddy-induced MOC (third column in Fig. 4). Thus, the eddy compensation can be reflected by the GM parameterized eddy transport regardless of the κ scheme. However, compared with the other four experiments, FMH4D has the most extensive enhancement and area of the anticlockwise eddy-induced MOC (third column in Fig. 4) among the five experiments. That largest eddy-induced MOC from FMH4D can reduce its residual MOC. But it is not the smallest, since the Eulerian MOC also plays an important role. The Eulerian MOC also shows sensitivity to κ despite the same change in wind stress. That may be caused by the secondary effects of κ, such as the isopycnal slope and the meridional density gradient. The choice of κ scheme shows the crucial role of κ in simulating the response of the MOC.

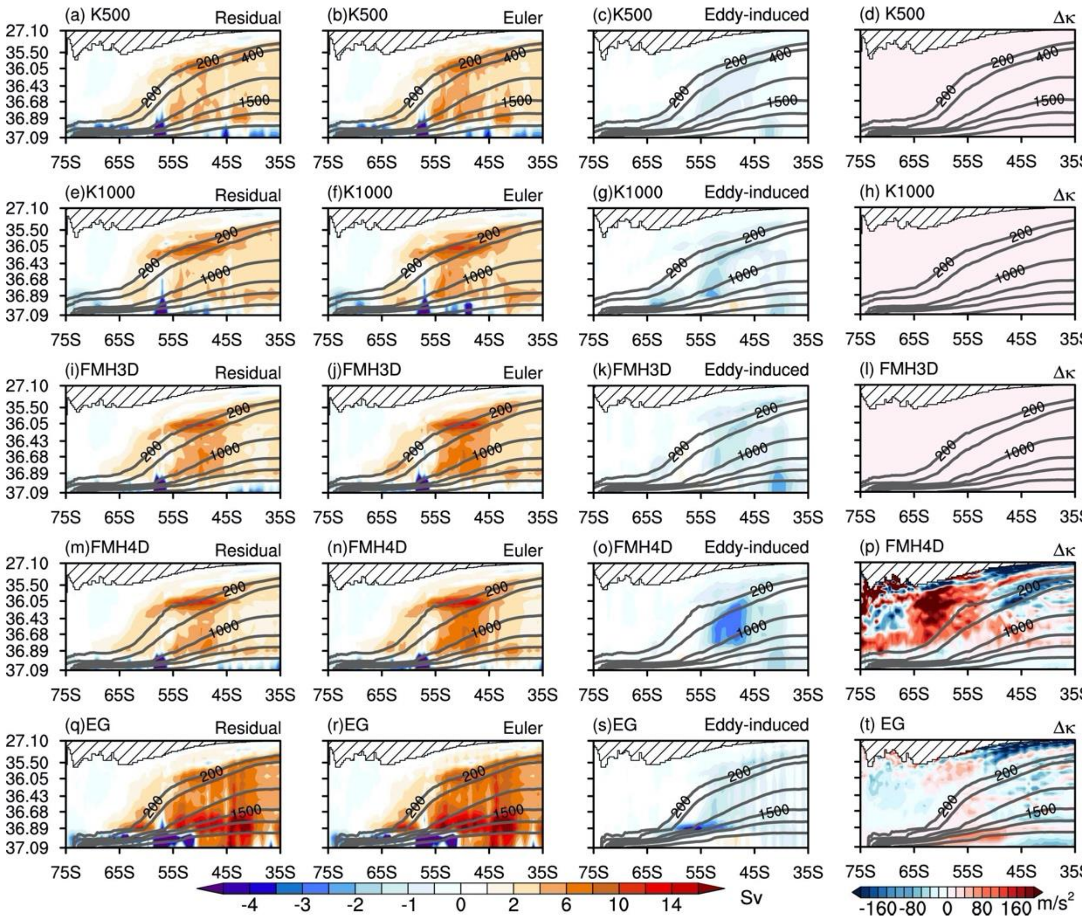

Figure 4. The first row is (a) the residual MOC, (b) the Eulerian MOC, (c) the eddy-induced MOC, and (d) the eddy transfer coefficient (Δκ) difference between 1960–1969 and 1998–2007 for the K500 experiment. The gray lines represent the zonally averaged isobaths (200, 400, 1000, 1500, 2000, and 3000 m) in the isopycnal coordinate system. The second to the bottom rows are for K1000, FMH3D, FMH4D, and EG experiments, respectively. (Unit: Sv)

To quantify the difference among the five experiments, we also use the defined indexes to measure the strength of the upper cell, which are the maximum value of the residual and Eulerian MOC and the minimum value of the eddy-induced MOC in the whole area. The changes in the residual, Eulerian, and eddy-induced MOC between 1960–1969 and 1998–2007 are listed in Table 2. The enhanced eddy compensation for LICOMH is -2.83 Sv. For the coarse-resolution experiments, the FMH4D and EG experiments have a relatively larger eddy compensation of -2.33 Sv and -1.68 Sv, respectively, which are closer to LICOMH. For the K500, K1000, and FMH3D experiments, the enhanced eddy-induced MOC is smaller, which is -0.41 Sv, -0.36 Sv, and -1.19 Sv, respectively. Thus, the spatiotemporal variance of κ is crucial to the eddy compensation regardless of the κ scheme.

Besides, the comparison between K500 and K1000 suggests that a smaller value of κ leads to a stronger eddy compensation response. The contrast between FMH3D and FMH4D indicates that the spatially varying κ is not sufficient to simulate the full compensation effect. Despite the spatiotemporally varying κ in FMH4D and EG, there is still a nonignorable different eddy compensation response between them. That implies the purely buoyancy-dependent κ leads to a stronger eddy compensation response than the time- and length-scale dependent κ.

Although the eddy compensation response is simulated in all five experiments, the absolute values of the response are all smaller than that in LICOMH. FMH4D has the largest eddy compensation response of −2.33 Sv, which accounts for 82% of LICOMH, whereas K500 only makes up 14% of LICOMH. Therefore, the parameterized eddy with buoyancy-dependent κ can simulate the major eddy compensation response in the eddy-resolving model. There is still at least 18% eddy compensation that cannot be simulated by the coarse-resolution experiments.

Table 2. The differences in the strength for the residual, Eulerian, and eddy-induced MOC between 1960–1969 and 1998–2007 for the high-resolution and five coarse-resolution experiments.

Experiments	**Residual**	**Eulerian**	**Eddy**

LICOMH	5.83	5.84	-2.84
K500	2.78	2.60	-0.41
K1000	3.19	3.57	-0.36
FMH3D	2.10	6.45	-1.19
FMH4D	1.88	6.54	-2.33
EG	5.35	4.78	-1.68

Note: The strength is the maximal positive value in the whole area for residual and Eulerian MOCs. And the strength for Eddy-induced MOC is the minimum value in the whole area. (Unit: Sv)

Based on the comparison above, we found that the coarse-resolution experiments are capable of capturing up to 82% of the eddy compensation response from the reference eddy-resolving experiment. The spatiotemporal variation of κ based on buoyancy is crucial in simulating the eddy compensation response. This was previously pointed out by Abernathey et al. (2011) through an idealized channel model. Our results indicate that the temporal variation of the buoyancy-dependent κ plays a more significant role in simulating the eddy compensation response than its spatial variation in a global coarse-resolution ocean-sea ice model. Nevertheless, further analysis is required to understand the effect of the spatiotemporal variation of the eddy transfer coefficient on the eddy compensation and why the temporal variation based on buoyancy is more important.

4. Influence on the eddy compensation

As shown above, we find that the eddy compensation from the FMH4D and EG experiments is closer to the high-resolution result, whereas the other experiments show weaker eddy compensation. In this section, we further analyze why the eddy transfer coefficients with spatiotemporal variations, especially the buoyancy dependent κ lead to stronger eddy-induced MOC enhancement.

4.1 The attribution of the eddy-induced MOC

The eddy-induced velocity in LICOML is parameterized following Gent and McWilliams (1990).

$$u^* = (\kappa \frac{\rho_x}{\rho_z})_z = (\kappa Slope\_x)_z \quad (11)$$

$$v^* = (\kappa \frac{\rho_y}{\rho_z})_z = (\kappa Slope\_y)_z \quad (12)$$

where u^* and v^* are the zonal and meridional eddy-induced velocity, respectively; κ is the eddy transfer coefficient; and ρ_x, ρ_y, and ρ_z are the partial differential of density in the zonal, meridional, and vertical directions, respectively. Therefore, ρ_x/ρ_z and ρ_y/ρ_z represent the zonal and meridional isopycnal slope, represented as $Slope\_x$ and $Slope\_y$.

If κ has vertical variation, the velocity can be decomposed into two terms. The meridional bolus velocity can be presented as:

$$v^* = (\kappa Slope\_y)_z = \kappa(Slope\_y)_z + Slope\_y\kappa_z \quad (13)$$

where the two terms on the right-hand side represent the impact of κ spatial structure (called SS hereafter) and the impact of the vertical variation of κ (called VV hereafter). The VV term is the newly introduced term owing to the vertical variation of κ, which will vanish in the constant scheme of κ. Those two artificial components are divergent, as their streamfunctions are not closed at the bottom (Fig. 5c-e and Fig. 6a-c). The terms for the five schemes used in this study are listed in Table 3. For the experiments with constant κ (K500 and K1000), their eddy-induced velocities only contain the SS part. The VV part vanishes due to the lack of vertical variation in κ. For experiments with spatially varying κ (FMH3D, FMH4D, and EG), their eddy-induced velocities contain both SS and VV. The responses of SS and VV for the five experiments are also listed in Table 3, which is described in Section 4.2.

Table 3. The components of the SS and VV terms among the five experiments, and the components of their response.

	SS	VV	ΔSS	ΔVV

K500	$\kappa(Slope\_y)_z$	-	$(Slope\_y)'_z\kappa$	-
K1000	$\kappa(Slope\_y)_z$	-	$(Slope\_y)'_z\kappa$	-
FMH3D	$\kappa(Slope\_y)_z$	$\kappa_z Slope\_y$	$(Slope\_y)'_z\kappa$	$(Slope\_y)'\kappa_z$
FMH4D	$\kappa(Slope\_y)_z$	$\kappa_z Slope\_y$	$(Slope\_y)'_z\kappa$ $+ (Slope\_y)_z\kappa'$ $+ (Slope\_y)'_z\kappa'$	$(Slope\_y)'\kappa_z$ $+ (Slope\_y)\kappa'_z$ $+ (Slope\_y)'\kappa'_z$
EG	$\kappa(Slope\_y)_z$	$\kappa_z Slope\_y$	$(Slope\_y)'_z\kappa$ $+ (Slope\_y)_z\kappa'$ $+ (Slope\_y)'_z\kappa'$	$(Slope\_y)'\kappa_z$ $+ (Slope\_y)\kappa'_z$ $+ (Slope\_y)'\kappa'_z$

Figure 5 shows the eddy-induced MOC due to the SS term among the five experiments during 1960–1969 and the changes between 1960–1969 and 1998–2007. The calculation is the same as equation (9) but based on the SS-induced velocity. The SS-induced MOC from the experiments with a constant scheme (K500 and K1000) is the whole eddy-induced MOC, which is a closed circulation (Fig. 5a and 5b). However, for the experiments with spatially varying κ, the values of the SS-induced MOC and their changes are all negative, which contributes to the eddy compensation. Based on the comparison among the five experiments in Figure 5, it is clear that the spatially varying κ leads to a stronger SS term than in the constant schemes. In addition, the temporal variation of κ leads to a stronger response of the eddy compensation compared with the spatially varying κ. The MOC strength for the two constant scheme experiments is around 10 Sv (Fig. 5a and 5b), whereas it is larger than 20 Sv for the FMH3D, FMH4D, and EG experiments (Fig. 5c–5e). Compared with the FMH3D scheme, the FMH4D and EG schemes have larger responses, which are larger than 4 Sv between 50°S and 55°S (Fig. 5i and 5j).

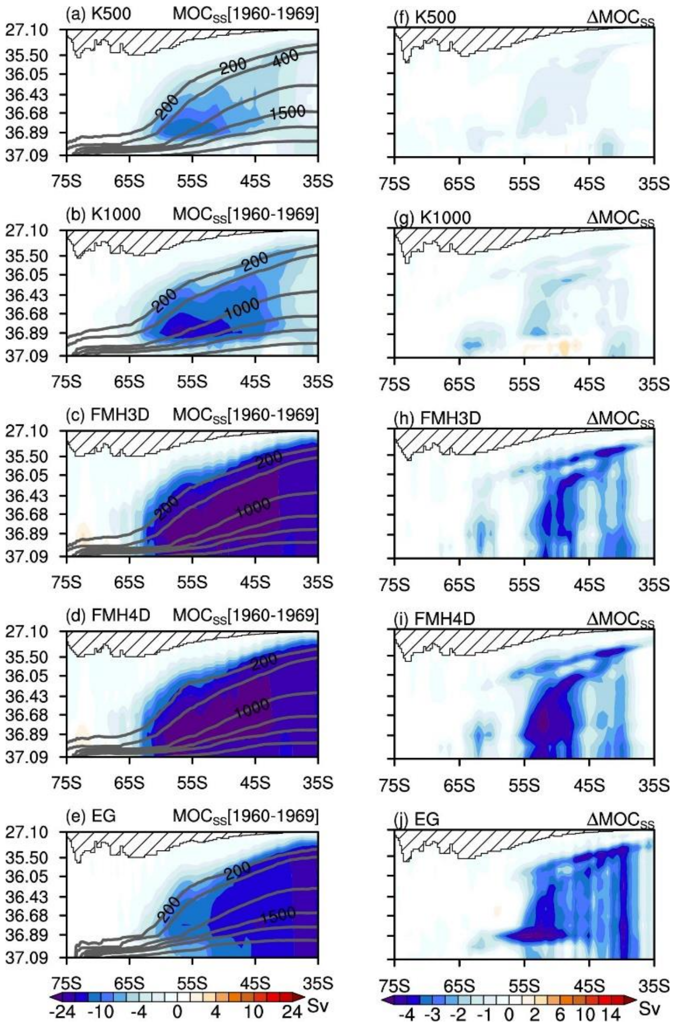

Figure 5. The left column is the SS-induced MOC during 1960–1969 for (a) K500, (b) K1000, (c) FMH3D, (d) FMH4D, and (e) EG. The right column is the difference in the SS-induced MOC between 1960–1969 and 1998–2007 for the five experiments. The gray lines in the left column are the zonally averaged isobaths (200, 400, 1000, 1500, 2000, and 3000 m) in the isopycnal coordinate system. (Unit: Sv)

Furthermore, the SS-induced MOC for the five schemes also has a different spatial structure. For the constant scheme, the centers of the MOC are located around 55°S and the surface of 36.89 kg m^{-3} with a maximum magnitude of 10 Sv for K500 and 18 Sv for K1000 (Fig. 5a and 5b), whereas the larger than 18 Sv center of the MOC can be found around 40°–60°S and 36.43–36.89 kg m^{-3} for the FMH3D and FMH4D (Fig. 5c and 5d) and south of 40°S and 36.05–36.89 kg m^{-3} for the EG experiment. In general, their responses occur between 50°S and 55°S (Fig. 5f and 5g), which are also the latitudes of the large wind-stress changes. These differences in the structure of the SS-induced response of the MOC are reflected in the response of the eddy-induced MOC

(Fig. 4c, 4g, 4k, 4o, and 4s).

Figure 6 shows the VV-induced MOC during 1960–1969 for experiments with spatially varying schemes and their responses to enhanced westerlies. If we compare the VV term with the SS term (Fig. 5), we find that the VV term and its response are always positive or a clockwise MOC, which compensates for the SS term and leads to a closed circulation. As the VV-induced MOC is opposite to the SS-induced MOC and the eddy-induced MOC, it is the SS term that dominates the eddy-induced MOC. The changes in the VV-induced MOC are all about 3 Sv, which is less than the changes in the SS-induced MOCS, which is about 4 Sv. Therefore, the total responses of the eddy-induced MOC are all approximately 1 Sv or less. The contrast between the SS- and the VV-induced MOC indicates that the eddy compensations for the FMH4D and EG experiments come from the enhanced SS-induced MOC, rather than the introduced VV-induced MOC derived from the vertical variation of κ.

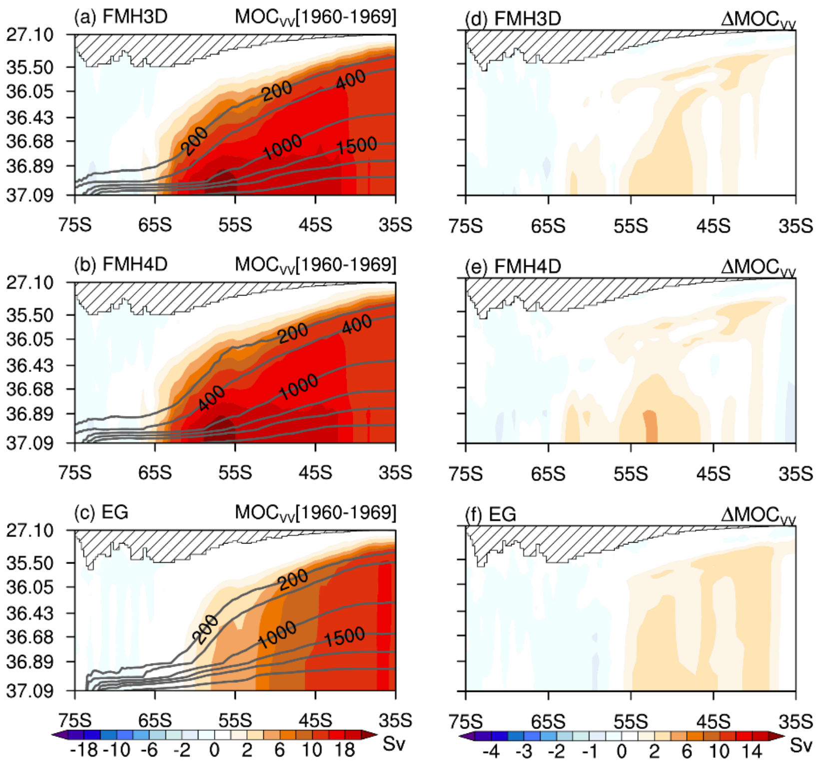

Figure 6. The left column is the VV-induced MOC during 1960–1969 for (a) FMH3D, (b) FMH4D, and (c) EG. The right column is the difference in the VV-induced MOC between 1960–1969 and 1998–2007 for the three experiments. The gray lines in the left column are the zonally averaged isobaths (200, 400, 1000, 1500,

2000, and 3000 m) in the isopycnal coordinate system. (Unit: Sv)

4.2 The attribution of the response

The decomposition of the eddy-induced MOC has revealed that the clockwise SS-induced MOC and anticlockwise VV-induced MOC contribute to eddy compensation. The SS and VV components are two components of the eddy-induced velocity resulting from a mathematical decomposition. They indicate the impact of the eddy transfer coefficient itself (SS) and its vertical variation (VV), respectively. To explore the attribution of the SS-induced and VV-induced MOC, Figure 7 illustrates the components of the SS and VV-induced MOCs, including the SS-induced velocity (V_{SS}), the VV-induced velocity (V_{VV}) and the thickness of the density layers (dz). Although the dz among the five experiments is similar, V_{SS} and V_{VV} exhibit significant differences, indicating that the variation in the SS and VV-induced MOC among the different experiments stems from the differences in V_{SS} and V_{VV}. Hence, it is valid to assess the attribution of the response of the SS and VV-induced MOCs through the SS and VV-induced velocities.

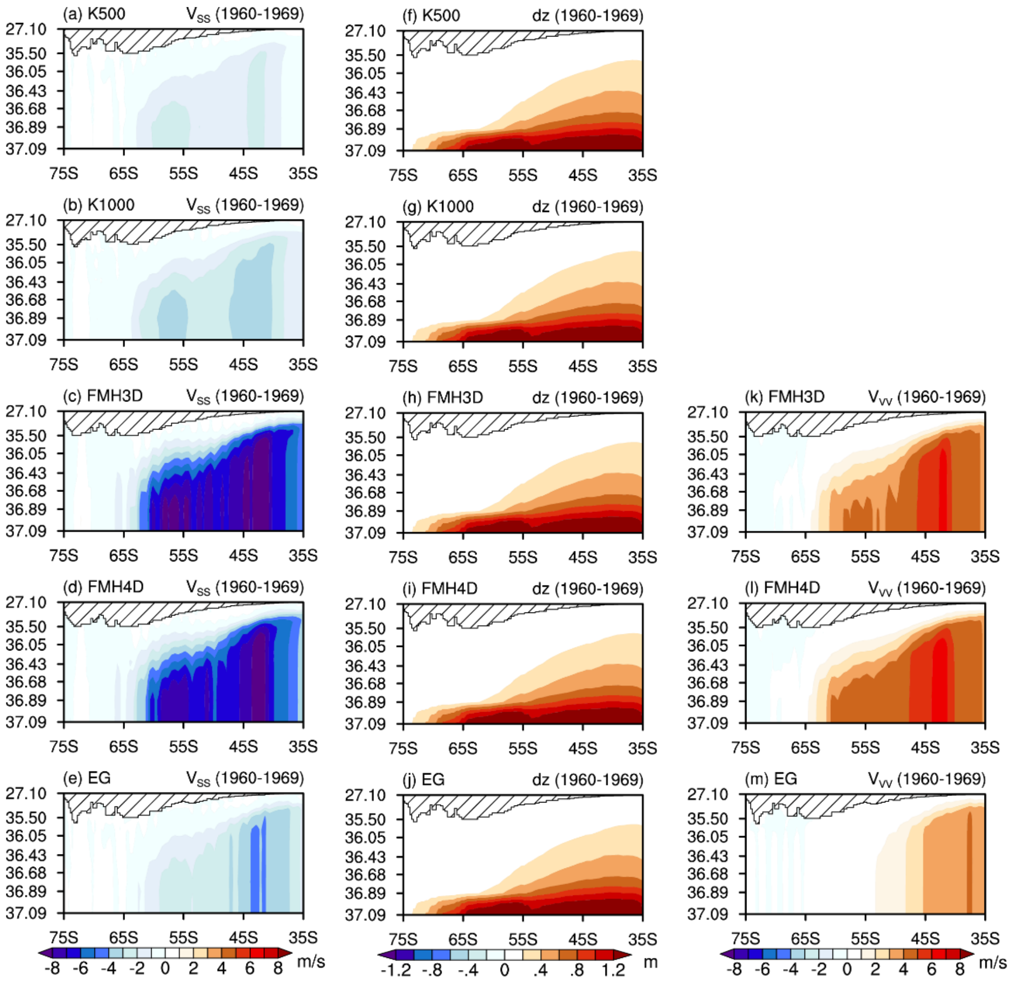

Figure 7. The left panels from top to bottom are the zonally integrated SS-induced velocities (m s^{-1}) during 1960–1969 for (a) K500, (b) K1000, (c) FMH3D, (d) FMH4D, and (e) EG. The middle panels (f)-(j) are the zonally integrated thicknesses of the density layers (dz) during 1960–1969 for the five experiments. The right panels are the zonally integrated VV-induced velocities (m s^{-1}) during 1960-1969 for (k) FMH3D, (l) FMH4D, and (m) EG.

Based on the decomposition of the eddy-induced velocity, the response of the SS term can also be decomposed as follows:

$$\begin{aligned}\Delta V_{SS}' &= V_{SS}(1998\text{-}2007) - V_{SS}(1960\text{-}1969) \\ &= (\kappa + \kappa')\,[(Slope\_y)_z + (Slope\_y)_z'] - \kappa(Slope\_y)_z \\ &= (Slope\_y)_z'\kappa + (Slope\_y)_z\kappa' + (Slope\_y)_z'\kappa' \qquad (14)\end{aligned}$$

where $\Delta V_{SS}'$ represents the difference between 1998–2007 averaged and 1960–1969 averaged SS-induced velocity. κ is the eddy transfer coefficient during 1960–1969 and κ' is the difference in κ between 1998–2007 and 1960–1969. $(Slope\_y)_z$ is the vertical partial derivative of the meridional isopycnal slope during 1960–1969 and $(Slope\_y)_z'$

is the difference of $(Slope\_y)_z$ between 1998–2007 and 1960–1969. The components of the decomposition from all five experiments are listed in Table 3. Even though the spatial and temporal variation of κ show a vital role in the SS-induced MOC, it is not clear whether the better simulations of the response of the eddy-induced MOC for the FMH4D and EG experiments come from κ itself or the isopycnal slope, which are two significant components of the eddy-induced velocity.

Figure 8 shows the responses of the SS-induced velocity and its components from the FMH4D and EG experiments. A comparison of the response of SS-induced velocity ($\Delta V'_{\mathrm{SS}}$) and its three components reveals that the value and pattern of $(Slope\_y)'_z\kappa$ are almost identical to $\Delta V'_{\mathrm{SS}}$ in both experiments. The spatial correlations between $(Slope\_y)'_z\kappa$ and $\Delta V'_{\mathrm{SS}}$ are 0.98 and 0.96, in FMH4D and EG, respectively. On average, the ratio of $(Slope\_y)'_z\kappa$ to $\Delta V'_{\mathrm{SS}}$ averaged over the whole region can reach 0.83 and 1.31, respectively. Conversely, the other two components ($(Slope\_y)_z\kappa'$ and $(Slope\_y)'_z\kappa'$) exhibit much smaller spatial correlations and ratios in both experiments. As such, the dominant component of $\Delta V'_{\mathrm{SS}}$ is $(Slope\_y)'_z\kappa$, which represents the response of the isopycnal slope and κ during the first decade. This highlights that the response of the isopycnal slope (the indirect impact of κ) plays the primary role in the response of the SS-induced MOC in experiments with spatiotemporally varying κ. This is because the GM parameterization is based on baroclinic instability and the change of isopycnal slopes can indicate the transfer of available potential energy (APE) into the eddy kinetic energy (EKE). Hence, for the parameterization of the eddy compensation response, the temporal variation of the isopycnal slope (indirect impact of κ) is more important than the direct response of κ.

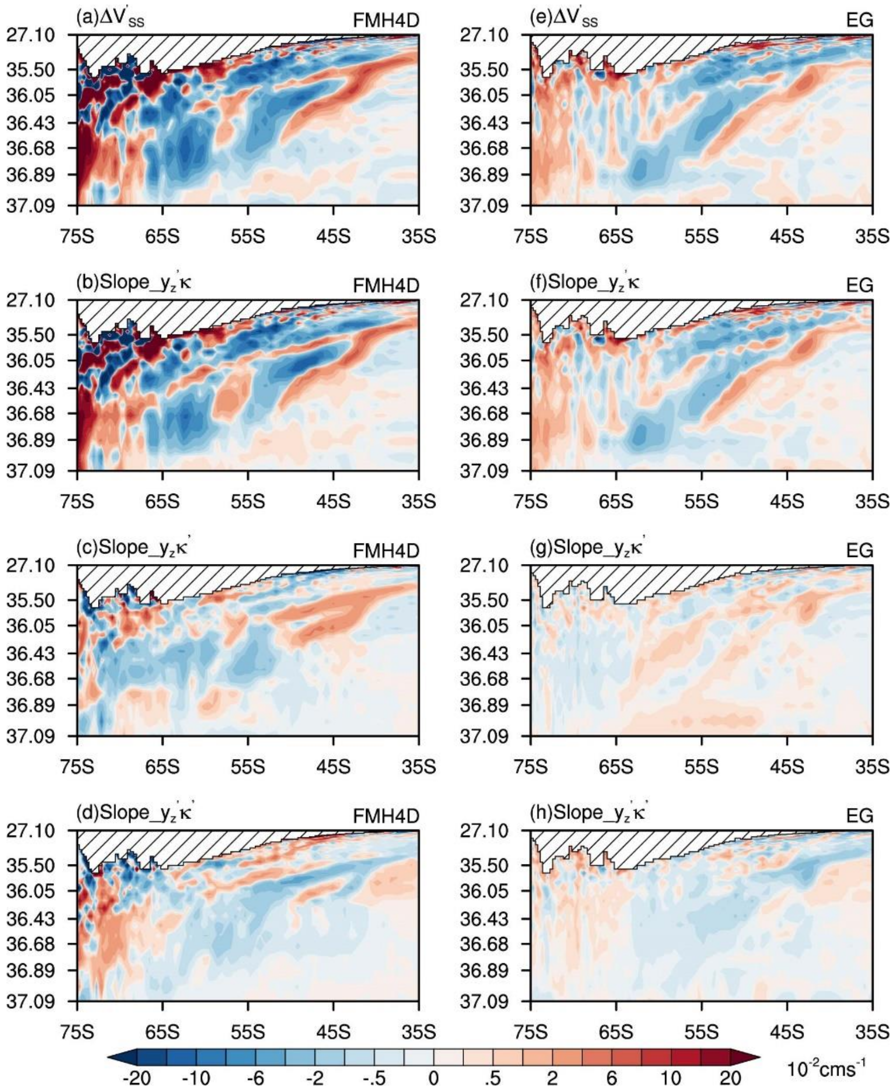

Figure 8. The left column is (a) the difference of the SS term-induced velocity ($\Delta V'_{SS}$) between 1960–1969 and 1998–2007 for the FMH4D experiment and its three components (b) $(Slope\_y)'_z\kappa$, (c) $(Slope\_y)_z\kappa'$ and (d) $(Slope\_y)'_z\kappa'$. The right column is the same as the left column, but for the EG experiment. (Unit: 10^{-2} cm s^{-1})

Although SS term-induced velocity contributes to the eddy compensation, the VV term-induced velocity is nonignorable for the final state of the eddy-induced MOC. The response of the VV term-induced velocity can be decomposed as follows:

$$\begin{aligned}\Delta V'_{VV} &= V_{VV}(1998\text{-}2007) - V_{SS}(1960\text{-}1969) \\ &= (Slope\_y + Slope\_y')(\kappa_z + \kappa_z') - (Slope\_y)\kappa_z \\ &= (Slope\_y)'\kappa_z + (Slope\_y)\kappa_z' + (Slope\_y)'\kappa_z' \qquad (15)\end{aligned}$$

where $\Delta V'_{VV}$ is the difference between 1998-2007 averaged (V_{VV}(1998-2007)) and 1960-1969 averaged VV-induced velocity (V_{VV}(1960-1969)). $Slope\_y$ is the meridional isopycnal slope during 1960–1969 and $(Slope\_y)'$ is the difference of $Slope\_y$

between 1998–2007 and 1960–1969. κ_z represent the vertical variation of the eddy transfer coefficient during 1960-1969 and $\kappa_z{}'$ is the difference of κ_z between 1998-2007 and 1960-1969. Thus, the response of the VV term-induced velocity consists of three terms, which are also listed in Table 3.

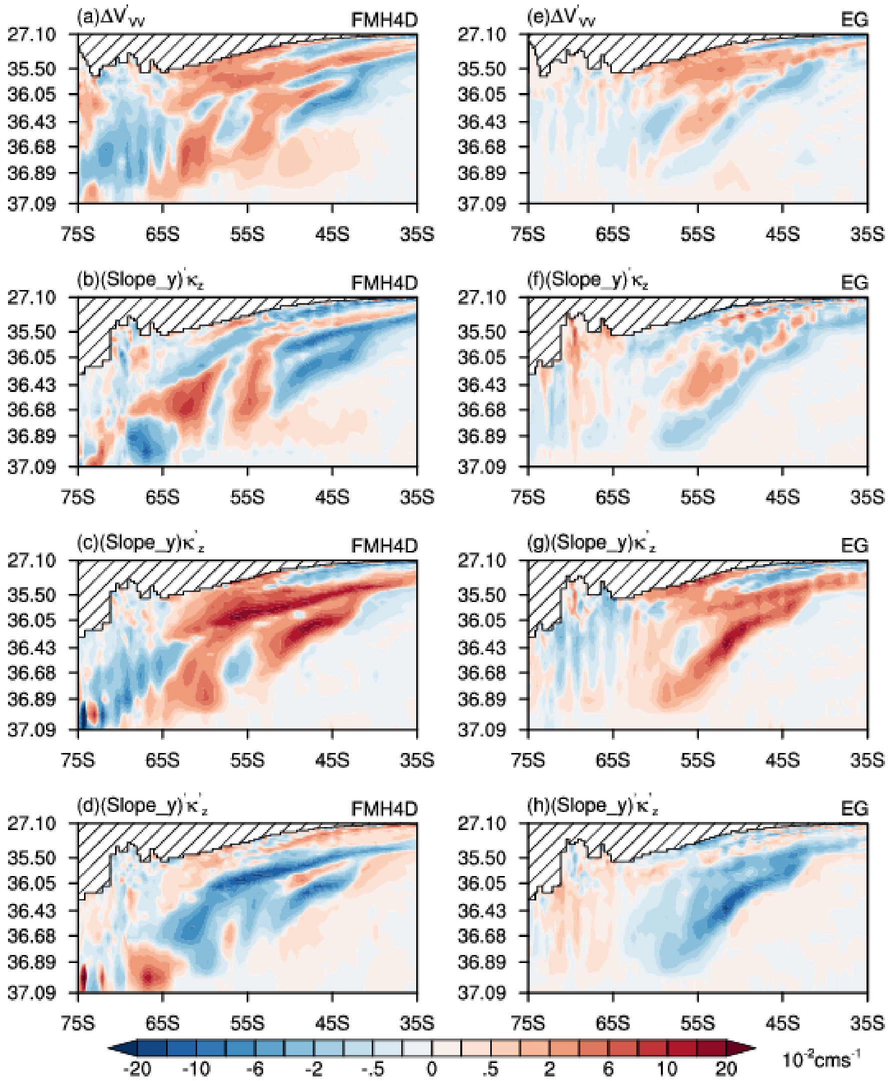

Figure 9. The left column is (a) the difference of the VV term-induced velocity ($\Delta V'_{\mathrm{VV}}$) between 1960–1969 and 1998–2007 for the FMH4D experiment and its three components (b) $(Slope\_y)'\kappa_z$, (c) $(Slope\_y)\kappa'_z$ and (d) $(Slope\_y)'\kappa'_z$. The right column is the same as the left column, but for the EG experiment. (Unit: 10^{-2} cm s^{-1})

Figure 9 displays the response of the VV term-induced velocity and its three components from FMH4D and EG. Different from the response of the SS-induced velocity, the response of the VV-induced velocity is determined by all three components. The spatial correlations between $(Slope\_y)'\kappa_z$ and $\Delta V'_{\mathrm{VV}}$ from FMH4D and EG are 0.51

and 0.27 respectively. The spatial correlations between $(Slope\_y)\kappa_z'$ and $\Delta V_{\mathrm{VV}}'$ are also small, and so are the correlations between $(Slope\_y)'\kappa_z'$ and $\Delta V_{\mathrm{VV}}'$ (Table 4). For the ratios of the three components to $\Delta V_{\mathrm{VV}}'$, all three components show nonnegligible ratios (Table 4). Based on the spatial correlations and ratios, all three components play an important role in the response of the VV-induced velocity, which is different from the SS-induced velocity. Thus, for the response of the VV part, which reduces the eddy compensation, there is no dominant factor, as the responses of both slope and κ make a large contribution to the response of VV-induced velocity.

Table 4 The spatial correlation coefficients between the change of SS-induced velocity ($\Delta V_{SS}'$) and its three components ($(Slope\_y)_z'\kappa$, $(Slope\_y)_z\kappa'$, $(Slope\_y)_z'\kappa'$) for FMH4D and EG. The spatial correlation coefficients between the change of VV-induced velocity ($\Delta V_{\mathrm{VV}}'$) and its three components ($(Slope\_y)'\kappa_z$, $(Slope\_y)\kappa_z'$, $(Slope\_y)'\kappa_z'$) for FMH4D and EG. The mean ratio in the whole region of the zonal averaged three components of $\Delta V_{SS}'$ ($\Delta V_{VV}'$) to $\Delta V_{SS}'$ ($\Delta V_{VV}'$) for FMH4D and EG.

Case	Components		Spatial Correlation		Ratio	
	SS	VV	SS	VV	SS	VV
FMH4D	$(Slope\_y)_z'\kappa$	$(Slope\_y')\kappa_z$	0.98	0.51	0.83	1.01×10^{17}
	$(Slope\_y)_z\kappa'$	$(Slope\_y)\kappa_z'$	0.54	0.28	0.07	6.10×10^{16}
	$(Slope\_y)_z'\kappa'$	$(Slope\_y')\kappa_z'$	-0.20	-0.19	0.03	-7.14×10^{16}
EG	$(Slope\_y)_z'\kappa$	$(Slope\_y')\kappa_z$	0.96	0.27	1.31	-97.55
	$(Slope\_y)_z\kappa'$	$(Slope\_y)\kappa_z'$	0.31	0.41	-0.49	672.97
	$(Slope\_y)_z'\kappa'$	$(Slope\_y')\kappa_z'$	-0.13	-0.09	0.33	-101.66

In summary, the response of the SS-induced MOC from the FMH4D and EG experiments, leading to stronger eddy compensation, can be traced back to the response of the isopycnal slope, despite the importance of κ. For experiments with non-temporally varying κ, the eddy compensation response is also traced back to the response of the isopycnal slope since κ is not varying with time.

4.3 The attribution of the isopycnal slope

As analyzed in section 3.4.2, the response of the isopycnal slope is the dominant factor leading to the SS-induced response, strengthening the eddy compensation in the

FMH4D and EG experiments. This implies that the change of the isopycnal slope with time is more important than the change of κ for the response of the eddy compensation, even though the temporal variation of κ is essential for the parameterization of the eddy compensation response.

Figure 10 shows the meridional isopycnal slope, the vertical variation of the meridional isopycnal slope during 1960–1969, and their responses from 1960–1969 to 1998–2007 among the five experiments. For the impact of the value of κ, a larger value leads to a smaller meridional isopycnal slope (comparing K1000 with K500, Fig. 10a and Fig. 10b). Furthermore, the value of κ has the same impact on the isopycnal slope (Fig. 10a and 10b), the vertical variation of the isopycnal slope (Fig. 10k and 10l), and their response (Fig. 10f and 10g; Fig. 10p and 10q).

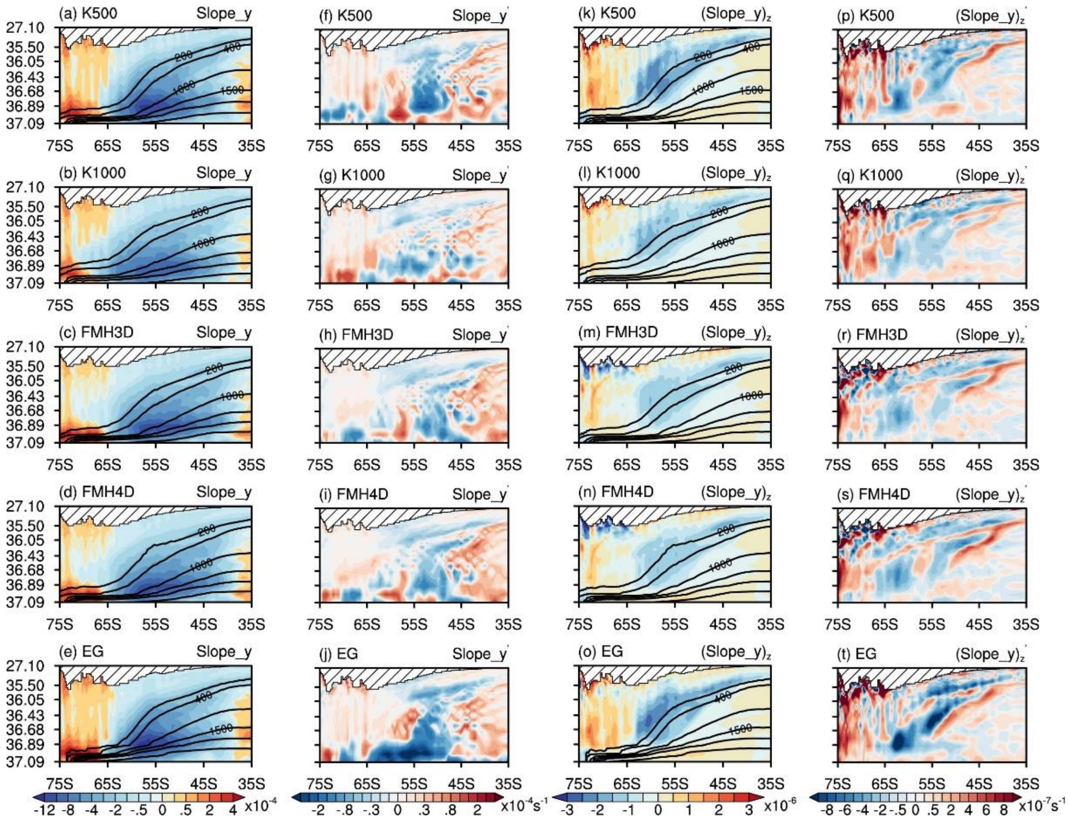

Figure 10. The zonal-averaged meridional isopycnal slope for (a) K500, (b) K1000, (c) FMH3D, (d) FMH4D, and (e) EG during 1960–1969. The difference in the zonal-averaged meridional isopycnal slopes between 1960–1969 and 1998–2007 for (f) K500, (g) K1000, (h) FMH3D, (i) FMH4D, and (j) EG. The zonal-averaged vertical variation of the meridional isopycnal slope for (k) K500, (l) K1000, (m) FMH3D, (n) FMH4D, and (o) EG. The difference in the zonal-averaged vertical variation of the

meridional isopycnal slope between 1960–1969 and 1998–2007 for (p) K500, (q) K1000, (r) FMH3D, (s) FMH4D, and (t) EG.

In experiments with constant κ, the response of the eddy-induced MOC has only one component, which contains κ and the change of the vertical variation of the isopycnal slope (Table. 3). With a smaller response of the slope's vertical variation (Fig. 10p and 10q), K1000 still has stronger eddy compensation than K500 (Table 2), which is caused by its larger value of κ. Thus, the different simulated eddy compensation response among cases with constant schemes is caused by the value of κ itself, rather than its secondary effect.

Comparing FMH4D with K500 (Fig. 10 first and fourth rows), the spatiotemporally varying κ leads to smaller changes of the isopycnal slope (Fig. 10i) and its vertical variation (Fig. 10s). That smaller change of the isopycnal slope means a more flattened slope in FMH4D than that in K500, since the response of the isopycnal slope is negative, which is caused by the enhanced westerlies. For the vertical variation of the isopycnal slope, which is the major factor for the response of SS-induced MOC, FMH4D shows a smaller value than K500. That means the stronger SS-induced eddy compensation response in FMH4D than K500 is due to the larger κ in FMH4D.

Comparing FMH4D with FMH3D (Fig. 10 third and fourth rows), the additional temporal variation of κ leads to a stronger enhancement of the isopycnal slope and its vertical variation. That stronger response of the slope's vertical variation contributes to the stronger eddy compensation in FMH4D (Table 2). Thus, the additional temporal variation of buoyancy-dependent κ strengthens the eddy compensation response through κ's secondary impact on the isopycnal slope's response.

The EG experiment shows a larger response of the isopycnal slope's vertical variation than FMH4D, even though the eddy compensation from EG is weaker than that from FMH4D (Table 2). The reason is that the larger response of the isopycnal slope's vertical variation not only causes the stronger response of the SS-induced velocity in EG but also leads to a stronger VV-induced velocity, which counteracts the effect of the SS term.

Thus, although the isopycnal slope's response is the primary factor in the parameterization of the eddy compensation response in all experiments, the different eddy compensation responses between constant κ and spatiotemporally varying κ come from κ directly. Only the additional temporally varying κ leads to a stronger eddy compensation response through the response of the isopycnal slope directly. To sum up, κ affects the eddy-induced velocity based on GM parameterization first. Then, the eddy-induced transports of heat and salinity change the distributions of the temperature and salinity globally, which affects the isopycnal slope. Besides, the affected surface temperature and salinity change the heat and freshwater flux at the surface, which affects the temperature and salinity, even the circulation. All those impacts can affect κ and the eddy-induced velocity in return, forming a positive cycle.

5. Summary and Discussion

In this study, we quantify the influence of five eddy transfer coefficients on the response of the Southern Ocean MOC to intensified westerlies in a non-eddy-resolving ocean model driven by CORE-II forcing. The results indicate that using a buoyancy frequency-based coefficient that varies both spatially and temporally leads to the closest simulation of the Southern Ocean MOC response to that of the reference eddy-resolving simulation. However, this parameterization can only replicate 82% of the eddy compensation response in the reference eddy-resolving model.

The study finds that the spatial and temporal variability in buoyancy-dependent κ leads to a six times stronger eddy compensation response than constant κ (5.7 times more than K500 and 6.5 times more than K1000). Despite the importance of the spatial and temporal variations of κ for simulating the eddy compensation response, the temporal variance of κ is more important than its spatial variance, as the eddy compensation response from FMH4D (-2.33 Sv) is two times stronger than that from FMH3D (-1.19 Sv). In addition, the contrast between FMH4D (-2.33 Sv) and EG (-1.68 Sv) highlights the importance of the buoyancy feature, represented by the baroclinic instability, as FMH4D is buoyancy-dependent and EG is controlled by several factors.

A full decomposition of the eddy-induced MOC and its respones in experiments with spatiotemporally varying κ indicates that the new term derived from the vertical variation of κ does not strengthen the eddy compensation but counteract it. And those enhanced eddy compensation responses are primarily attributed to the response of the isopycnal slope, which is also the major part of the eddy compensation response in experiments with constant κ. Hence, the introduction of the spatiotemporal variation of κ does not change the major contribution to the eddy compensation response. The impact of κ on the eddy-induced velocity based on the GM parameterization and its subsequent effects on the temperature and salinity distributions, surface heat and freshwater flux, and circulation all form a positive feedback cycle.

The results of this study indicate that stratification- and scale-based schemes that allow for spatial and temporal variability in κ improve the simulation of the Southern Ocean MOC's response to climate change. However, it is important to note that the strength of the residual MOC and the Eulerian MOC still show substantial differences between the LICOMH and the five coarse-resolution experiments, which may be due to differences in buoyancy flux and sea ice coupling. As such, it is necessary to evaluate the eddy compensation in various eddy-resolving models to gain a more realistic reference for coarse-resolution climate ocean models.

Acknowledgments

Drs. Li, Liu, Lin, and Yu are supported by National Key R&D Program for Developing Basic Sciences (2018YFA0605703, 2016YFC1401401, 2016YFC1401601) and the National Natural Science Foundation of China (Grants 41931183). Dr. Chassignet is supported by the CAS President's International Fellowship Initiative (PIFI) and NOAA

Climate Program Office MAPP Program (Award NA15OAR4310088). The data used in this paper can be downloaded from https://osf.io/nr4yf/.

References

Abernathey, R. P., & Ferreira, D. (2015). Southern Ocean isopycnal mixing and ventilation changes driven by winds, Geophys. Res. Lett., 42, 10,357–10,365, doi:10.1002/2015GL066238.

Abernathey, R. P., & Marshall, J. (2013). Global surface eddy diffusivities derived from satellite altimetry. Journal of Geophysical Research: Oceans, 118(2), 901-916. https://doi.org/10.1002/jgrc.20066

Abernathey, R.P., Marshall, J., & Ferreira, D. (2011). The dependence of Southern Ocean meridional overturning on wind stress. Journal of Physical Oceanography, 41(12), 2261-2278.

Bishop, S. P., Gent, P. R., Bryan, F. O., Thompson, A. F., Long, M. C., & Abernathey, R. (2016). Southern Ocean overturning compensation in an eddy-resolving climate simulation. Journal of Physical Oceanography, 46(5), 1575-1592. https://doi.org/10.1175/JPO-D-15-0177.1

Böning, C. W., Dispert, A., Visbeck, M., Rintoul, S. R., & Schwarzkopf, F. U. (2008). The response of the Antarctic Circumpolar Current to recent climate change. Nature Geoscience, 1(12), 864-869.

Bracegirdle, T. J., Shuckburgh, E., Sallee, J. B., Wang, Z., Meijers, A. J., Bruneau, N., ... & Wilcox, L. J. (2013). Assessment of surface winds over the Atlantic, Indian, and Pacific Ocean sectors of the Southern Ocean in CMIP5 models: Historical bias, forcing response, and state dependence. Journal of Geophysical Research: Atmospheres, 118(2), 547-562. https://doi.org/10.1002/jgrd.50153

Danabasoglu, G., & Marshall, J. (2007). Effects of vertical variations of thickness diffusivity in an ocean general circulation model. Ocean Modelling, 18(2), 122-141.

Doddridge, E. W., Marshall, J., Song, H., Campin, J.-M., Kelley, M., & Nazarenko, L. S. (2019). Eddy compensation dampens Southern Ocean sea surface temperature response to westerly wind trends. Geophysical Research Letters, 46, 4365– 4377

Downes, S. M., & Hogg, A. M. (2013). Southern Ocean circulation and eddy compensation in CMIP5 models. Journal of Climate, 26(18), 7198-7220.

Downes, S. M., Spence, P., & Hogg, A. M. (2018). Understanding variability of the Southern Ocean overturning circulation in CORE-II models. Ocean Modelling, 123, 98-109. https://doi.org/10.1016/j.ocemod.2018.01.005

Eden, C., & Greatbatch, R. J. (2008). Towards a mesoscale eddy closure. Ocean Modelling, 20(3), 223-239. https://doi.org/10.1016/j.ocemod.2007.09.002

Eden, C., Jochum, M., & Danabasoglu, G. (2009). Effects of different closures for thickness diffusivity. Ocean Modelling, 26(1-2), 47-59. https://doi.org/10.1016/j.ocemod.2008.08.004

Farneti, R., Downes, S. M., Griffies, S. M., Marsland, S. J., Behrens, E., Bentsen, M., ... & Canuto, V. M. (2015). An assessment of Antarctic Circumpolar Current and Southern Ocean meridional overturning circulation during 1958–2007 in a suite of interannual CORE-II simulations. Ocean Modelling, 93, 84-120. https://doi.org/10.1016/j.ocemod.2015.07.009

Ferreira, D., Marshall, J., & Heimbach, P. (2005). Estimating eddy stresses by fitting dynamics to observations using a residual-mean ocean circulation model and its adjoint. Journal of Physical Oceanography, 35(10), 1891-1910. https://doi.org/10.1175/JPO2785.1

Gent, P. R. (2016). Effects of Southern Hemisphere wind changes on the meridional overturning circulation in ocean models. Annual review of marine science, 8, 79-94. https://doi.org/10.1146/annurev-marine-122414-033929

Gent, P. R., & Danabasoglu, G. (2011). Response to increasing Southern Hemisphere winds in CCSM4. Journal of climate, 24(19), 4992-4998. https://doi.org/10.1175/JCLI-D-10-05011.1

Gent, P. R., & Mcwilliams, J. C. (1990). Isopycnal mixing in ocean circulation models. Journal of Physical Oceanography, 20(1), 150-155. https://doi.org/10.1175/1520-0485(1990)020<0150:IMIOCM>2.0.CO;2

Goyal, R., Gupta, A. S., Jucker, M., & England, M. H. (2021). Historical and projected changes in the Southern Hemisphere surface westerlies. Geophysical Research Letters, 48, e2020GL090849. https://doi.org/10.1029/2020GL090849

Hallberg, R., & Gnanadesikan, A. (2006). The role of eddies in determining the structure and response of the wind-driven Southern Hemisphere overturning: Results from the Modeling Eddies in the Southern Ocean (MESO) project. Journal of Physical Oceanography, 36(12), 2232-2252. https://doi.org/10.1175/JPO2980.1

Hofmann, M., & Morales Maqueda, M. A. (2011). The response of Southern Ocean eddies to increased midlatitude westerlies: A non-eddy resolving model study. Geophysical Research Letters, 38(3). https://doi.org/10.1029/2002GL015919

Large, W. G., & Yeager, S. G. (2004). Diurnal to decadal global forcing for ocean and sea-ice models: the data sets and flux climatologies. NCAR Technical Note. National Center for Atmospheric Research, 11, 324-336. https://doi.org/10.5065/D6KK98Q6

Large, W. G., & Yeager, S. G. (2009). The global climatology of an interannually varying air–sea flux data set. Climate dynamics, 33(2-3), 341-364. https://doi.org/10.1007/s00382-008-0441-3

Levitus, S., and T. P. Boyer (1994). World Ocean Atlas 1994, vol. 4, Temperature, NOAA Atlas NESDIS 4, 129 pp., Natl. Oceanic and Atmos. Admin., Silver Spring, Md.

Laurent, S., L. C., Simmons, H., & Jayne, S. (2002). Estimating tidally driven mixing in the deep ocean. Geophys. Res. Lett., 29, 21-1–21-4, doi: 10.1029/2002GL015633.

Li, Y., Liu, H., Ding, M., Lin, P., Yu, Z., Yu, Y., ... & Chen, K. (2020). Eddy-resolving

Simulation of CAS-LICOM3 for Phase 2 of the Ocean Model Intercomparison Project. Advances in Atmospheric Sciences, 37(10), 1067-1080.
Lin, P., Yu, Z., Liu, H., Yu, Y., Li, Y., Jiang, J., Xue, W., Chen, K., Yang, Q., Zhao, B. and Wei, J. (2020). LICOM Model Datasets for the CMIP6 Ocean Model Intercomparison Project. Advances in Atmospheric Sciences, 37(3), pp.239-249.
Liu, H., Lin, P., Yu, Y., & Zhang, X. (2012). The baseline evaluation of LASG/IAP climate system ocean model (LICOM) version 2. Acta Meteorologica Sinica, 26(3), 318-329. https://doi.org/10.1007/s13351-012-0305-y
Liu, H., Yu, Y., Lin, P., & Wang, F. (2014). High-resolution LICOM. In Flexible Global Ocean-Atmosphere-Land System Model (pp. 321-331). Springer, Berlin, Heidelberg. https://doi.org/10.1007/978-3-642-41801-3_38
Marshall, G. J. (2003). Trends in the Southern Annular Mode from observations and reanalyses. Journal of Climate, 16(24), 4134-4143. https://doi.org/10.1175/1520-0442(2003)016<4134:TITSAM>2.0.CO;2
Marshall, J., Scott, J. R., Romanou, A., Kelley, M., & Leboissetier, A. (2017). The dependence of the ocean's MOC on mesoscale eddy diffusivities: A model study. Ocean Modelling, 111, 1-8.
Meredith, M. P., Naveira Garabato, A. C., Hogg, A. M., & Farneti, R. (2012). Sensitivity of the overturning circulation in the Southern Ocean to decadal changes in wind forcing. Journal of Climate, 25(1), 99-110. https://doi.org/10.1175/2011JCLI4204.1
Miller, R. L., Schmidt, G. A., & Shindell, D. T. (2006). Forced annular variations in the 20th century intergovernmental panel on climate change fourth assessment report models. Journal of Geophysical Research: Atmospheres, 111(D18). doi:10.1029/2005JD006323
Munday, D. R., Johnson, H. L., & Marshall, D. P. (2013). Eddy saturation of equilibrated circumpolar currents. Journal of Physical Oceanography, 43(3), 507-532. https://doi.org/10.1175/JPO-D-12-095.1
Murray, R. J. (1996). Explicit generation of orthogonal grids for ocean models. Journal of Computational Physics, 126(2), 251-273. https://doi.org/10.1006/jcph.1996.0136
Poulsen, M. B., Jochum, M., & Nuterman, R. (2018). Parameterized and resolved Southern Ocean eddy compensation. Ocean Modelling, 124, 1-15. https://doi.org/10.1016/j.ocemod.2018.01.008
Redi, M. H. (1982). Oceanic Isopycnal Mixing by Coordinate Rotation, Journal of Physical Oceanography, 12(10), 1154-1158.
Smith, R. D., & Gent, P. R. (2004). Anisotropic Gent–McWilliams parameterization for ocean models. Journal of Physical Oceanography, 34(11), 2541-2564. https://doi.org/10.1175/JPO2613.1
Swart, N. C., & Fyfe, J. C. (2012). Observed and simulated changes in the Southern Hemisphere surface westerly wind-stress. Geophysical Research Letters, 39(16). https://doi.org/10.1029/2012GL052810
Swart, N. C., Fyfe, J. C., Saenko, O. A., & Eby, M. (2014). Wind-driven changes in the ocean carbon sink. Biogeosciences, 11(21), 6107-6117. DOI: 10.5194/bg-11-

6107-2014
Thompson, D. W., & Solomon, S. (2002). Interpretation of recent Southern Hemisphere climate change. Science, 296(5569), 895-899. DOI: 10.1126/science.1069270
Viebahn, J., & Eden, C. (2010). Towards the impact of eddies on the response of the Southern Ocean to climate change. Ocean Modelling, 34(3-4), 150-165.
Visbeck M, Marshall J, Haine T, Spall M. (1997) Specification of Eddy Transfer Coefficients in Coarse-Resolution Ocean Circulation Models. Journal of Physical Oceanography, 27(3):381-402.
Waugh, D. W. (2014). Changes in the ventilation of the southern oceans. Philosophical Transactions of the Royal Society A: Mathematical, Physical and Engineering Sciences, 372(2019), 20130269.
Yu, Y., Liu, H., & Lin, P. (2012). A quasi-global 1/10 eddy-resolving ocean general circulation model and its preliminary results. Chinese Science Bulletin, 57(30), 3908-3916. https://doi.org/10.1007/s11434-012-5234-8

Figure Captions

Figure 1. (a) The black line is the 12-month running mean zonal wind stress averaged in the Southern Ocean (40°S–60°S and 0–360°E) from LICOML. The thick black line is the linear trend of the monthly series. (b) The differences of the zonal wind stress from LICOML between periods of 1998–2007 and 1960–1969, and the zonally averaged values. The red solid and blue dashed lines are for 1960–1969 and 1998–2007, respectively.

Figure 2. The first column is the MOC of residual currents for the periods of (a) 1949–2007, (d) 1960–1969, (g) 1998–2007, and (j) the difference between 1998–2007 and 1960–1969 for LICOMH in the isopycnal coordinate. The black curves represent the zonally averaged isobaths (200, 400, 1000, 1500, 2000, and 3000 m) in the isopycnal coordinate. The second and third columns are the same as the first column, but for the Eulerian MOC and the eddy-induced MOC, respectively. The black numbers in the first and second columns are the maximum of the closed residual and Eulerian MOC. The white numbers in the third column are the minimum of the eddy-induced MOC. (Unit: Sv)

Figure 3. The top panels are (a) the residual MOC, (b) the Eulerian MOC, (c) the eddy-induced MOC, and (d) the eddy transfer coefficient (κ) for the K500 experiment during 1948–2009. The second to the bottom rows are the same as the first row, but for the K1000, FMH3D, FMH4D, and EG experiments, respectively. The gray lines represent the zonally averaged isobaths (200, 400, 1000, 1500, 2000, and 3000 m) in the isopycnal coordinate system. The black numbers in the first and second columns are the maximum of the residual and Eulerian MOC. The white numbers in the third column are the minimum of the eddy-induced MOC. (Unit: Sv)

Figure 4. The first row is (a) the residual MOC, (b) the Eulerian MOC, (c) the eddy-induced MOC, and (d) the eddy transfer coefficient (Δκ) difference between 1960–1969

and 1998–2007 for the K500 experiment. The gray lines represent the zonally averaged isobaths (200, 400, 1000, 1500, 2000, and 3000 m) in the isopycnal coordinate system. The second to the bottom rows are for K1000, FMH3D, FMH4D, and EG experiments, respectively. (Unit: Sv)

Figure 5. The left column is the SS-induced MOC during 1960–1969 for (a) K500, (b) K1000, (c) FMH3D, (d) FMH4D, and (e) EG. The right column is the difference in the SS-induced MOC between 1960–1969 and 1998–2007 for the five experiments. The gray lines in the left column are the zonally averaged isobaths (200, 400, 1000, 1500, 2000, and 3000 m) in the isopycnal coordinate system. (Unit: Sv)

Figure 6. The left column is the VV-induced MOC during 1960–1969 for (a) FMH3D, (b) FMH4D, and (c) EG. The right column is the difference in the VV-induced MOC between 1960–1969 and 1998–2007 for the three experiments. The gray lines in the left column are the zonally averaged isobaths (200, 400, 1000, 1500, 2000, and 3000 m) in the isopycnal coordinate system. (Unit: Sv)

Figure 7. The left panels from top to bottom are the zonally integrated SS-induced velocities (m s^{-1}) during 1960–1969 for (a) K500, (b) K1000, (c) FMH3D, (d) FMH4D, and (e) EG. The middle panels (f)-(j) are the zonally integrated thicknesses of the density layers (dz) during 1960–1969 for the five experiments. The right panels are the zonally integrated VV-induced velocities (m s^{-1}) during 1960-1969 for (k) FMH3D, (l) FMH4D, and (m) EG.

Figure 8. The left column is (a) the difference of the SS term-induced velocity ($\Delta V'_{\mathrm{SS}}$) between 1960–1969 and 1998–2007 for the FMH4D experiment and its three components (b) $(Slope\_y)'_z\kappa$, (c) $(Slope\_y)_z\kappa'$ and (d) $(Slope\_y)'_z\kappa'$. The right column is the same as the left column, but for the EG experiment. (Unit: 10^{-2} cm s^{-1})

Figure 9. The left column is (a) the difference of the VV term-induced velocity ($\Delta V'_{\mathrm{VV}}$)

between 1960–1969 and 1998–2007 for the FMH4D experiment and its three components (b) $(Slope\_y)'\kappa_z$, (c) $(Slope\_y)\kappa_z'$ and (d) $(Slope\_y)'\kappa_z'$. The right column is the same as the left column, but for the EG experiment. (Unit: 10^{-2} cm s^{-1})

Figure 10. The zonal-averaged meridional isopycnal slope for (a) K500, (b) K1000, (c) FMH3D, (d) FMH4D, and (e) EG during 1960–1969. The difference in the zonal-averaged meridional isopycnal slopes between 1960–1969 and 1998–2007 for (f) K500, (g) K1000, (h) FMH3D, (i) FMH4D, and (j) EG. The zonal-averaged vertical variation of the meridional isopycnal slope for (k) K500, (l) K1000, (m) FMH3D, (n) FMH4D, and (o) EG. The difference in the zonal-averaged vertical variation of the meridional isopycnal slope between 1960–1969 and 1998–2007 for (p) K500, (q) K1000, (r) FMH3D, (s) FMH4D, and (t) EG.

Figure S1. (a) The black line is the 12-month running mean zonal wind stress averaged in the Southern Ocean (40°S–60°S and 0–360°E) from LICOML (FMH4D is chosen here). The thick black line is the linear trend of the monthly series. The red line and the thick red line are the same as the black line and the thick black line but for LICOMH.

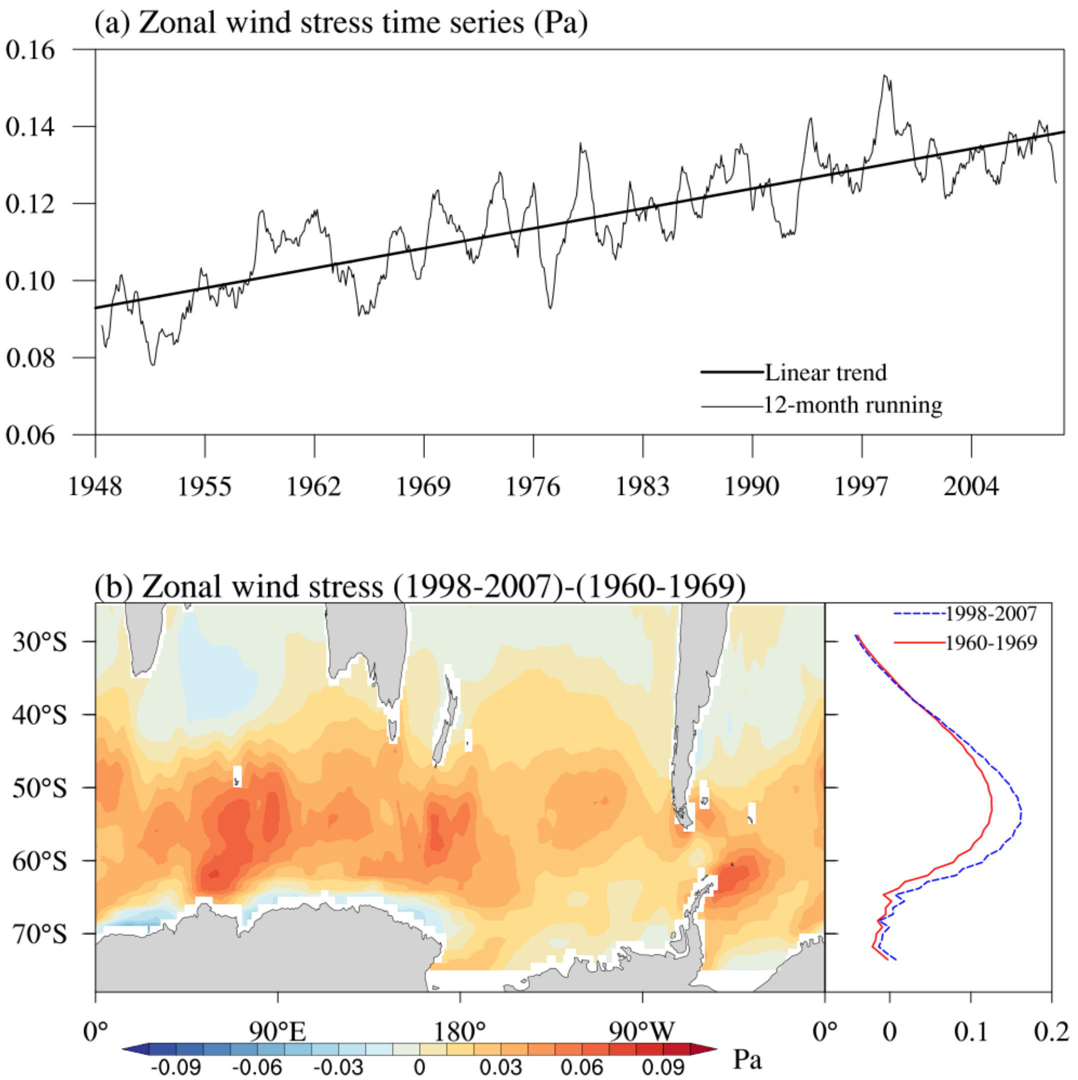

Figure 1. (a) The black line is the 12-month running mean zonal wind stress averaged in the Southern Ocean (40°S–60°S and 0–360°E) from LICOML. The thick black line is the linear trend of the monthly series. (b) The differences of the zonal wind stress from LICOML between periods of 1998–2007 and 1960–1969, and the zonally averaged values. The red solid and blue dashed lines are for 1960–1969 and 1998–2007, respectively.

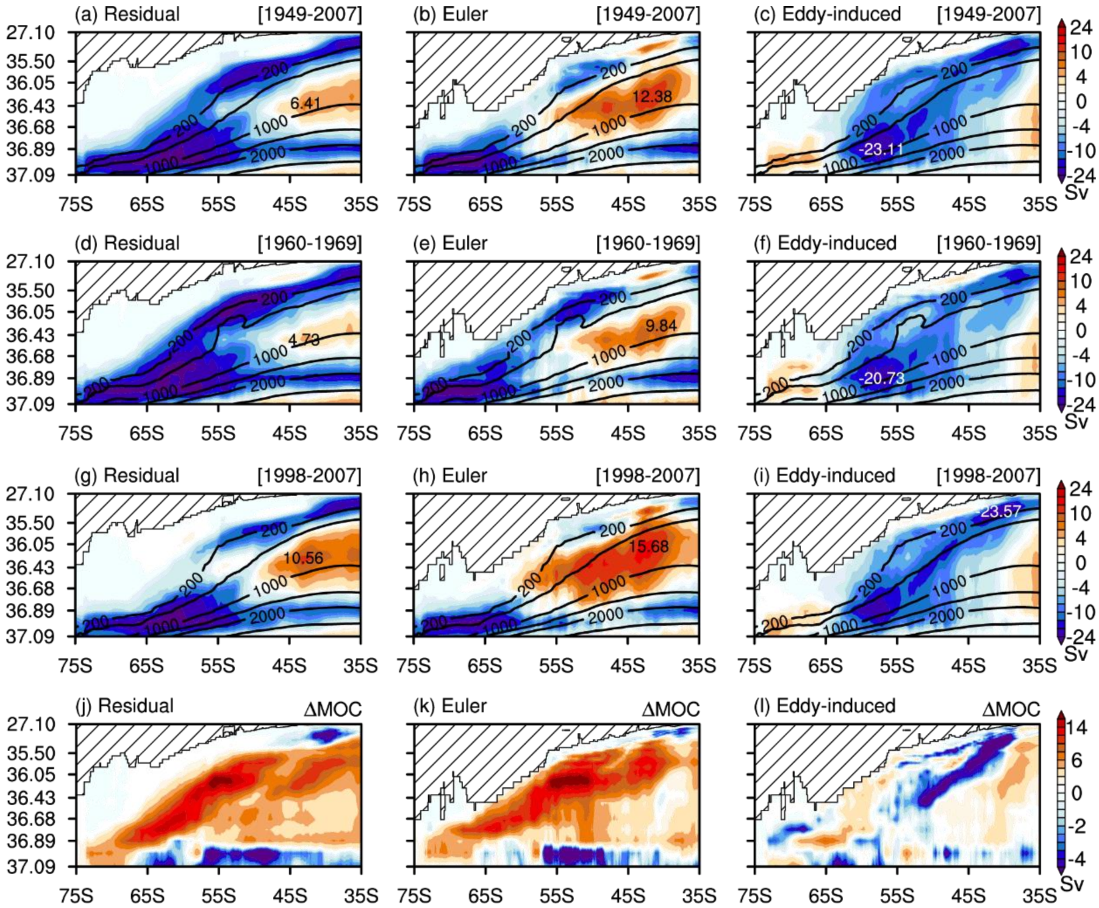

Figure 2. The first column is the MOC of residual currents for the periods of (a) 1949–2007, (d) 1960–1969, (g) 1998–2007, and (j) the difference between 1998–2007 and 1960–1969 for LICOMH in the isopycnal coordinate. The black curves represent the zonally averaged isobaths (200, 400, 1000, 1500, 2000, and 3000 m) in the isopycnal coordinate. The second and third columns are the same as the first column, but for the Eulerian MOC and the eddy-induced MOC, respectively. The black numbers in the first and second columns are the maximum of the closed residual and Eulerian MOC. The white numbers in the third column are the minimum of the eddy-induced MOC. (Unit: Sv)

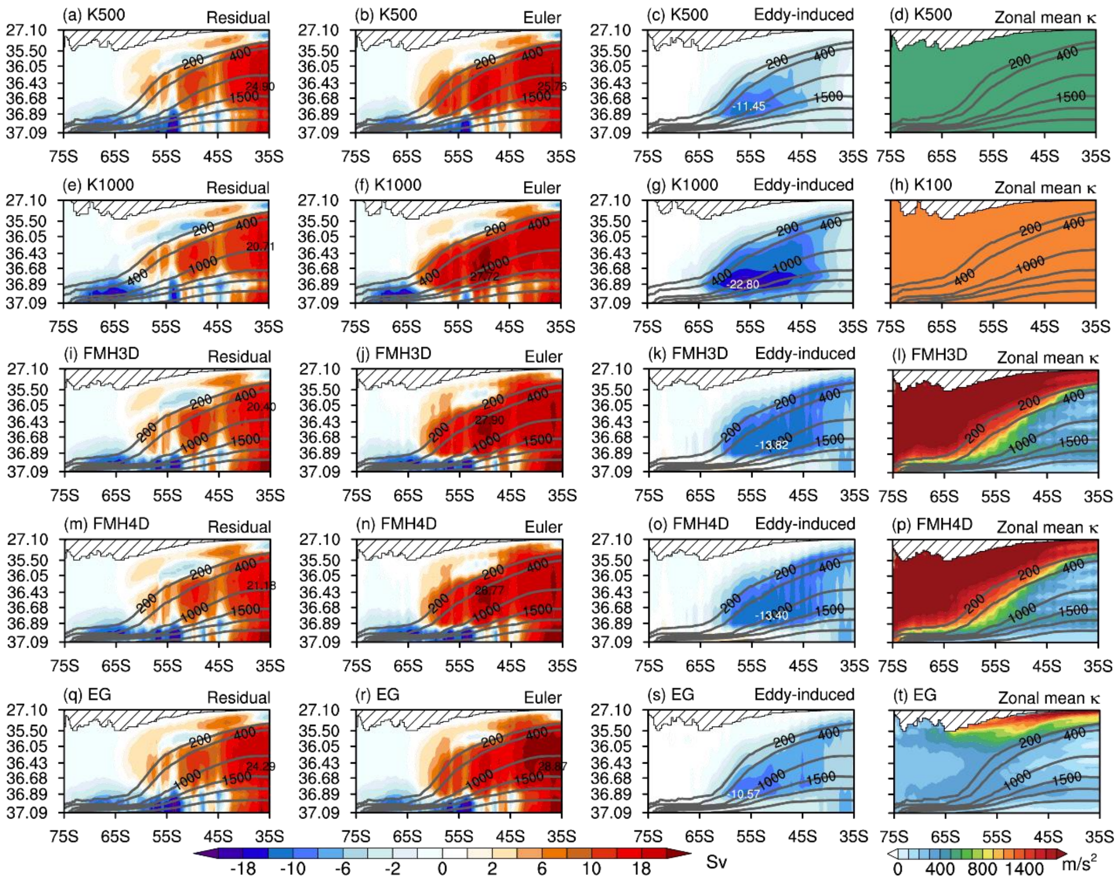

Figure 3. The top panels are (a) the residual MOC, (b) the Eulerian MOC, (c) the eddy-induced MOC, and (d) the eddy transfer coefficient (κ) for the K500 experiment during 1948–2009. The second to the bottom rows are the same as the first row, but for the K1000, FMH3D, FMH4D, and EG experiments, respectively. The gray lines represent the zonally averaged isobaths (200, 400, 1000, 1500, 2000, and 3000 m) in the isopycnal coordinate system. The black numbers in the first and second columns are the maximum of the residual and Eulerian MOC. The white numbers in the third column are the minimum of the eddy-induced MOC. (Unit: Sv)

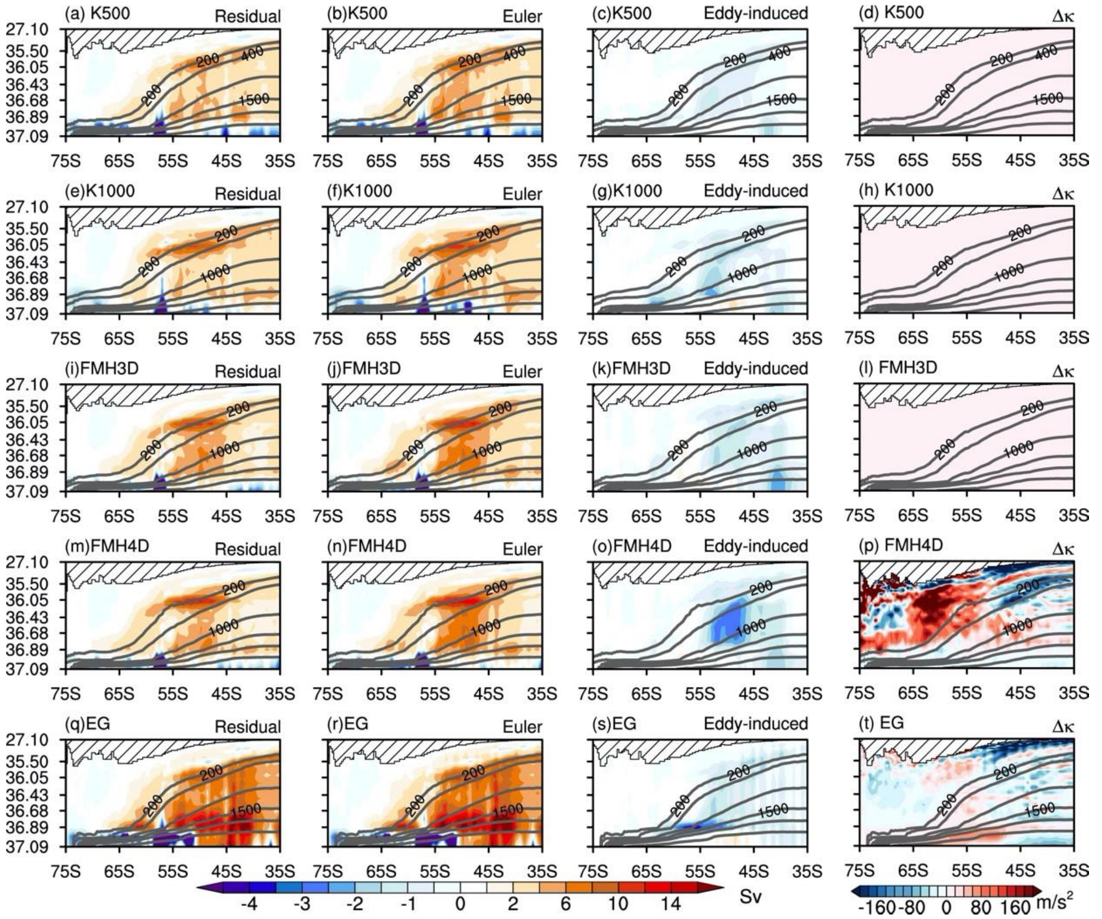

Figure 4. The first row is (a) the residual MOC, (b) the Eulerian MOC, (c) the eddy-induced MOC, and (d) the eddy transfer coefficient (Δκ) difference between 1960–1969 and 1998–2007 for the K500 experiment. The gray lines represent the zonally averaged isobaths (200, 400, 1000, 1500, 2000, and 3000 m) in the isopycnal coordinate system. The second to the bottom rows are for K1000, FMH3D, FMH4D, and EG experiments, respectively. (Unit: Sv)

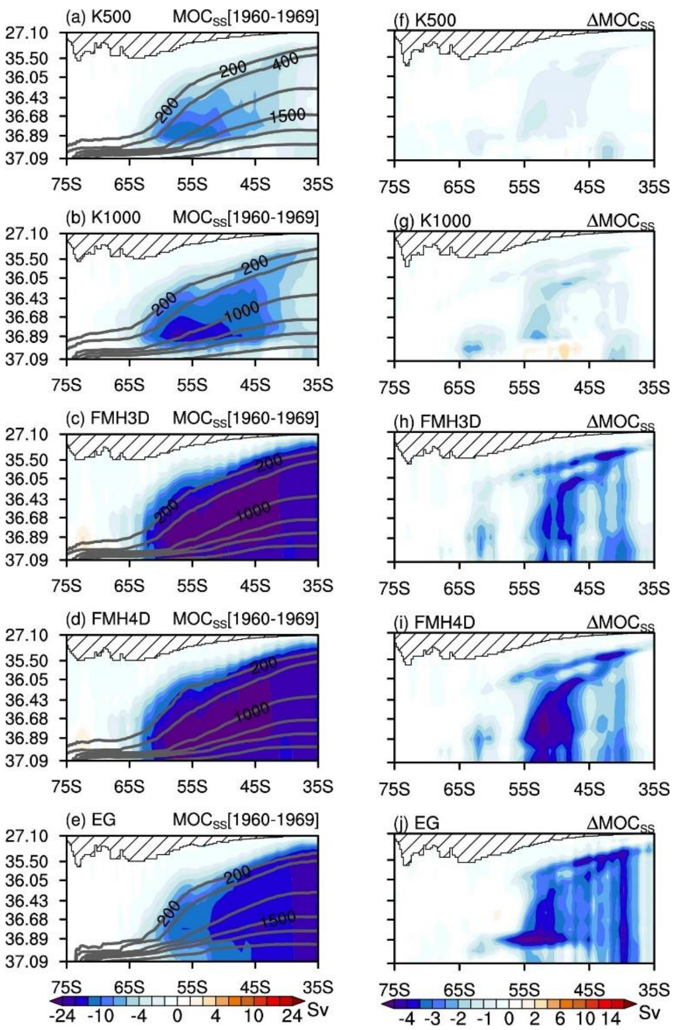

Figure 5. The left column is the SS-induced MOC during 1960–1969 for (a) K500, (b) K1000, (c) FMH3D, (d) FMH4D, and (e) EG. The right column is the difference in the SS-induced MOC between 1960–1969 and 1998–2007 for the five experiments. The gray lines in the left column are the zonally averaged isobaths (200, 400, 1000, 1500, 2000, and 3000 m) in the isopycnal coordinate system. (Unit: Sv)

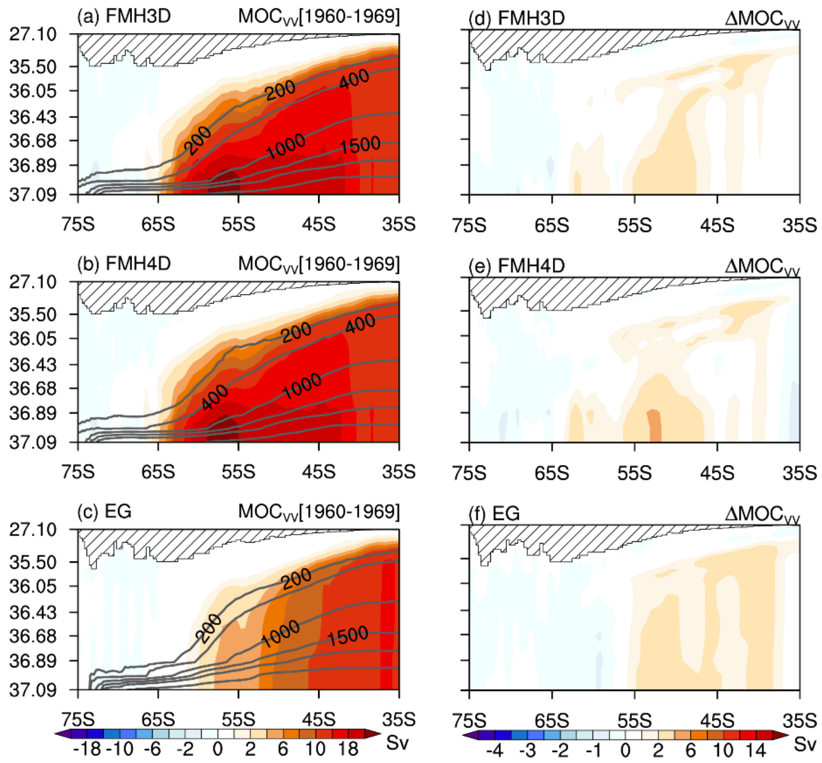

Figure 6. The left column is the VV-induced MOC during 1960–1969 for (a) FMH3D, (b) FMH4D, and (c) EG. The right column is the difference in the VV-induced MOC between 1960–1969 and 1998–2007 for the three experiments. The gray lines in the left column are the zonally averaged isobaths (200, 400, 1000, 1500, 2000, and 3000 m) in the isopycnal coordinate system. (Unit: Sv)

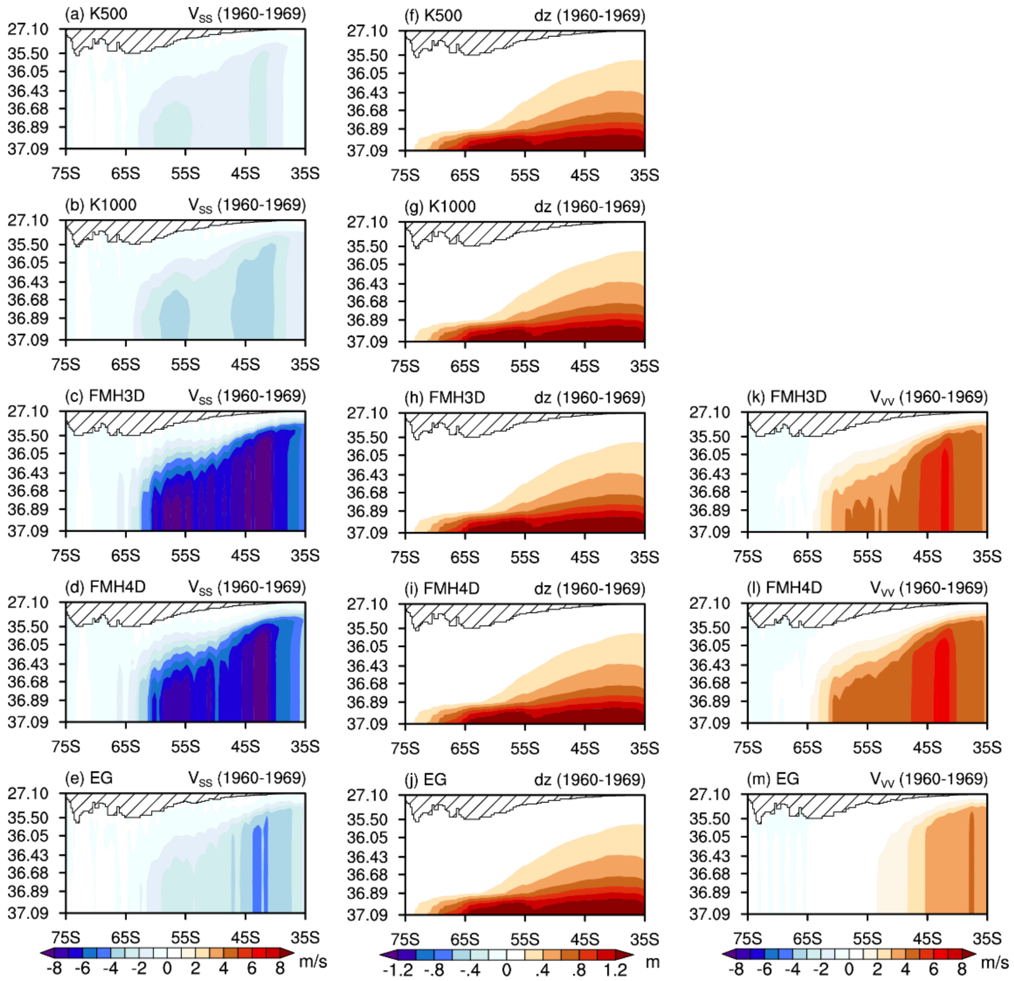

Figure 7. The left panels from top to bottom are the zonally integrated SS-induced velocities (m s^{-1}) during 1960–1969 for (a) K500, (b) K1000, (c) FMH3D, (d) FMH4D, and (e) EG. The middle panels (f)-(j) are the zonally integrated thicknesses of the density layers (dz) during 1960–1969 for the five experiments. The right panels are the zonally integrated VV-induced velocities (m s^{-1}) during 1960-1969 for (k) FMH3D, (l) FMH4D, and (m) EG.

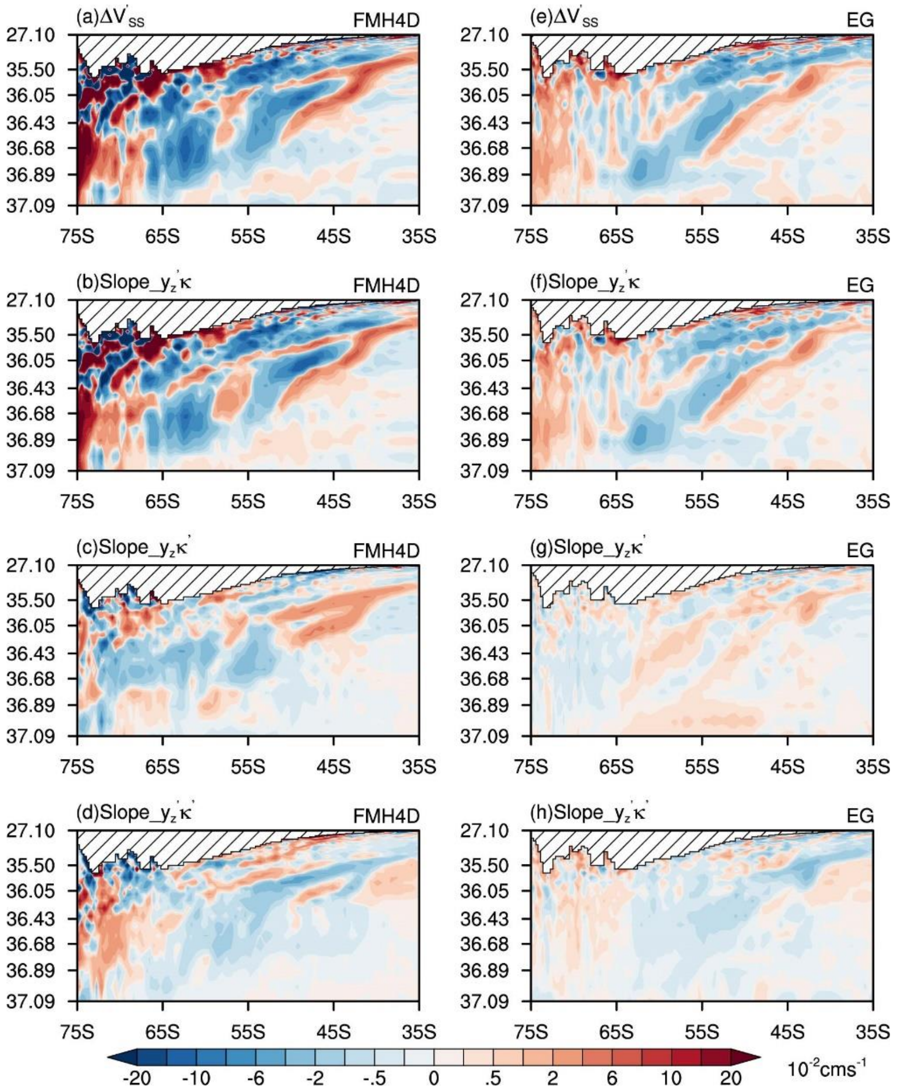

Figure 8. The left column is (a) the difference of the SS term-induced velocity ($\Delta V_{\mathrm{SS}}'$) between 1960–1969 and 1998–2007 for the FMH4D experiment and its three components (b) $(Slope\_y)_z'\kappa$, (c) $(Slope\_y)_z\kappa'$ and (d) $(Slope\_y)_z'\kappa'$. The right column is the same as the left column, but for the EG experiment. (Unit: 10^{-2} cm s^{-1})

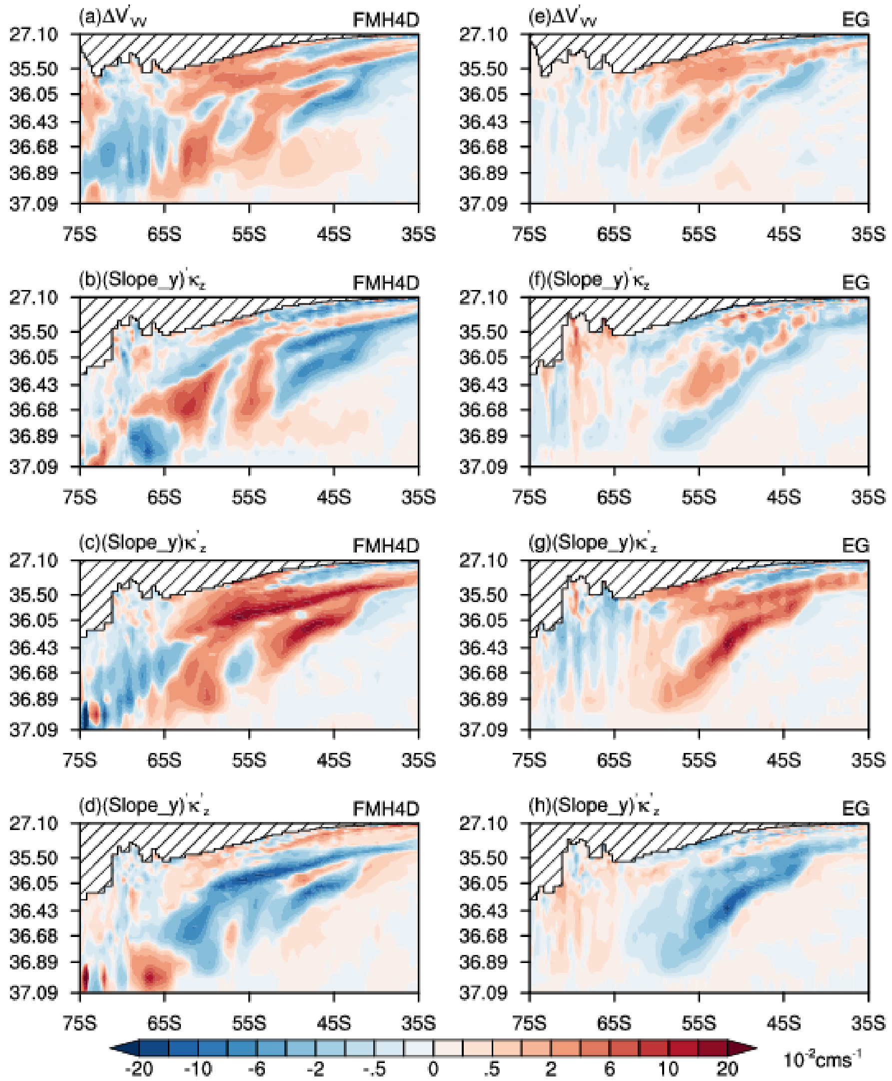

Figure 9. The left column is (a) the difference of the VV term-induced velocity ($\Delta V'_{\mathrm{VV}}$) between 1960–1969 and 1998–2007 for the FMH4D experiment and its three components (b) $(Slope\_y)'\kappa_z$, (c) $(Slope\_y)\kappa'_z$ and (d) $(Slope\_y)'\kappa'_z$. The right column is the same as the left column, but for the EG experiment. (Unit: 10^{-2} cm s^{-1})

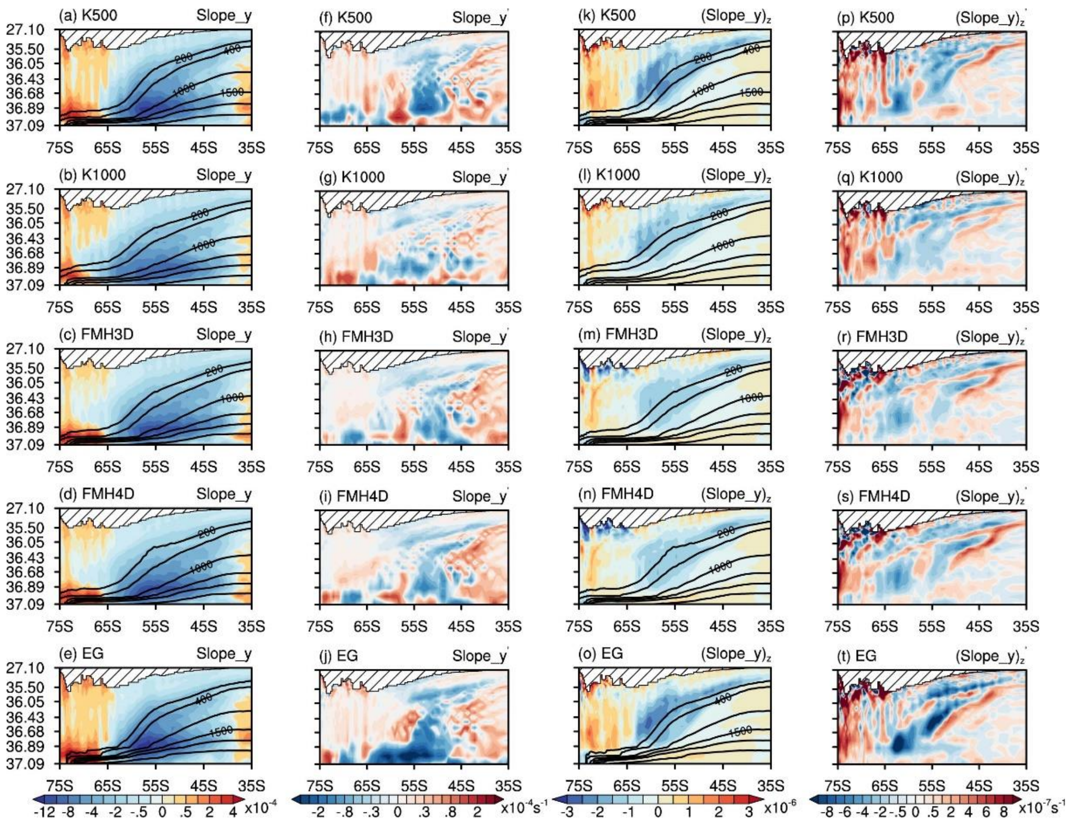

Figure 10. The zonal-averaged meridional isopycnal slope for (a) K500, (b) K1000, (c) FMH3D, (d) FMH4D, and (e) EG during 1960–1969. The difference in the zonal-averaged meridional isopycnal slopes between 1960–1969 and 1998–2007 for (f) K500, (g) K1000, (h) FMH3D, (i) FMH4D, and (j) EG. The zonal-averaged vertical variation of the meridional isopycnal slope for (k) K500, (l) K1000, (m) FMH3D, (n) FMH4D, and (o) EG. The difference in the zonal-averaged vertical variation of the meridional isopycnal slope between 1960–1969 and 1998–2007 for (p) K500, (q) K1000, (r) FMH3D, (s) FMH4D, and (t) EG.

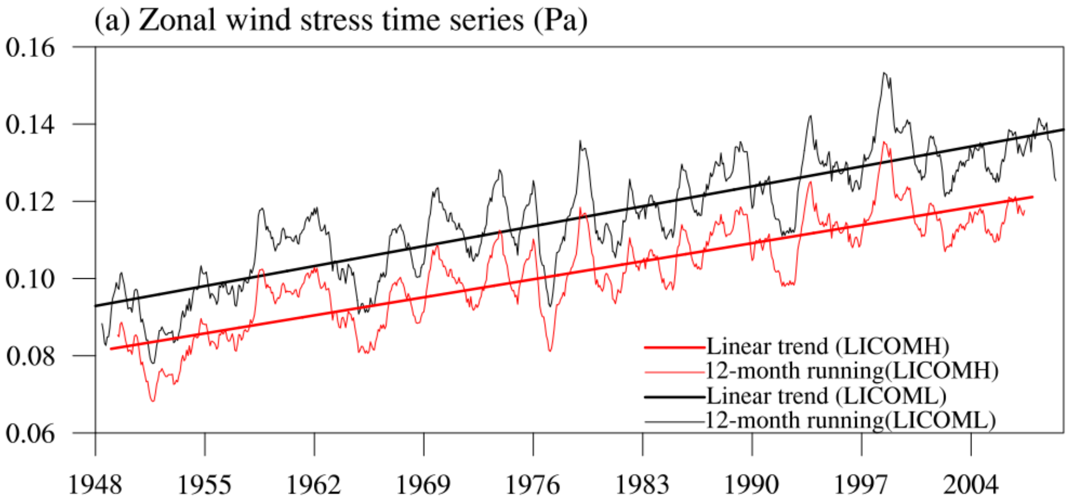

Figure S1. (a) The black line is the 12-month running mean zonal wind stress averaged in the Southern Ocean (40°S–60°S and 0–360°E) from LICOML (FMH4D is chosen here). The thick black line is the linear trend of the monthly series. The red line and the thick red line are the same as the black line and the thick black line but for LICOMH.